Stony Brook University

GaSb-based Type-I Diode Lasers Operating at 3 μm and above

A Dissertation Presented

by

Takashi Hosoda

to

The Graduate School

in Partial Fulfillment of the

Requirements

for the Degree of

Doctor of Philsophy

in

Electrical Engineering

Stony Brook University

December 2011

Stony Brook University
The Graduate School

Takashi Hosoda

We, the dissertation committee for the above candidate for the
Doctor of Philosophy degree, hereby recommend
acceptance of this dissertation.

Gregory Belenky – Dissertation Advisor
Distinguished Professor, Department of Electrical and Computer Engineering

Leon Shterengas – Co-Advisor of Dissertation
Assistant Professor, Department of Electrical and Computer Engineering

Milutin Stanacevic - Chairperson of Defense
Associate Professor, Department of Electrical and Computer Engineering

Mikhail Gouzman
Adjunct Professor, Department of Electrical and Computer Engineering

Alexander Orlov
Assistant Professor, Department of Materials Science and Engineering

This dissertation is accepted by the Graduate School

Lawrence Martin
Dean of the Graduate School

Abstract of the Dissertation

GaSb-based Type-I Diode Lasers Operating at 3 μm and above

by

Takashi Hosoda

Doctor of Philosophy

in

Electrical Engineering

Stony Brook University

2011

The ultimate goal of the research is the development of the semiconductor lasers operating at room temperature under continuous wave regime at 3 μm and above. This dissertation focuses on room temperature operated GaSb-based type-I diode lasers.

The new device design was proposed to reach desirable laser operation wavelength. Besides employing the compressively strained quantum wells (QWs) in the devices active region, the composition of waveguide and barrier material has been modified to optimize the band offsets between quantum wells and the neighboring layers. The use of quinternary AlGaInAsSb alloys for waveguide and barrier layers, leads to the reduction of conduction band offset and the increase of valence band offset between barrier and QWs in the device active region.

The comprehensive study of the characteristics of the devices with different waveguide widths, compositions, and the number of QWs allows us to design and

fabricate GaSb-based type-I lasers with world record performance. At room temperature in continuous wave (CW) mode, devices provide 360 mW at 3.0 μm; 190 mW at 3.1 μm; 165 mW at 3.2 μm; 50 mW at 3.3 μm; 16 mW at 3.4 μm.

Table of Contents

List of illustrations

List of tables

Publication

Journals:

1 T. Hosoda, G. Kipshidze, L. Shterengas, G. Belenky, “Single spatial mode 3 μm diode lasers with continuous wave output power of 15 mW at room temperature”, Electron. Lett., vol. 47, no. 24, pp. 1341-1343 (2011).

2 G. Belenky, L. Shterengas, G. Kipshidze, T. Hosoda, "Type-I diode lasers for spectral region above 3 μm", IEEE J. Sel. Topics Quantum Electron., vol. 17, no. 5, pp. 1426-1434 (2011).

3 G. Kipshidze, T. Hosoda, W. L. Sarney, L. Shterengas, G. Belenky, "High-power 2.2-μm diode lasers with metamorphic arsenic-free heterostructures", IEEE Photon. Technol. Lett., vol. 23, no. 5, pp. 317-319 (2011).

4 T. Hosoda, G. Kipshidze, L. Shterengas, G. Belenky, "Diodes lasers emitting near 3.44 μm in continuous wave regime at 300K", Electron. Lett., vol. 46, no. 21, pp. 1455-1456 (2010).

5 T. Hosoda, G. Kipshidze, G. Tsvid, L. Shterengas, G. Belenky, "Type-I GaSb-based laser diodes operating in 3.1-3.3 μm wavelength range", IEEE Photon. Technol. Lett., vol. 22, no. 10, pp. 718-720 (2010).

6 J. Chen, T. Hosoda, G. Kipshidze, L. Shterengas, G. Belenky, A. Soibel, C. Frez, S. Forouhar, "Single spatial mode room temperature operated 3.15 μm diode lasers", Electron. Lett., vol. 46, no. 5, pp. 367-368 (2010).

7 D. A. Firsov, L. Shterengas, G. Kipshidze, V. L. Zerova, T. Hosoda, P. Thumrongsilapa, L. E. Vorobjev, G. Belenky, "Dynamics of photoluminescence and recombination processes in Sb-containing laser nanostructures", Semiconductors, vol. 44, no. 1 pp. 50-58 (2010).

8 L. E. Vorob'ev, V. L. Zerova, D. A. Firsov, G. Belenky, L. Shterengas, G. Kipshidze, T. Hosoda, S. Suchalkin, M. Kisin, "Charge carrier recombination mechanisms in Sb-containing quantum well laser structures", Bulletin of the Russian Academy of Sciences: Physics, vol. 74, no. 1, pp. 69-71 (2010).

9 L. Shterengas, G. Kipshidze, T. Hosoda, J. Chen, G. Belenky, "Diode lasers emitting at 3 μm with 300 mW of continuous-wave output power", Electron. Lett., vol. 45, no. 18, pp. 942-943 (2009).

10 J. Chen, G. Kipshidze, L. Shterengas, T. Hosoda, Y. Wang, D. Donetsky, G. Belenky, "2.7 μm GaSb-based diode lasers with quinary waveguide", IEEE Photon. Technol. Lett., vol. 21, no. 16, pp. 1112-1114 (2009).

11 T. Hosoda, G. Kipshidze, L. Shterengas, S. Suchalkin, G. Belenky, "200 mW type-I GaSb-based laser diodes operating at 3 μm: role of waveguide width", Appl. Phys. Lett., vol. 94, p. 261104 (2009).

12 S. Suchalkin, S. Jung, G. Kipshidze, L. Shterengas, T. Hosoda, D. Westerfeld, D. Snyder, G. Belenky, "GaSb based light emitting diodes with strained InGaAsS type I quantum well active regions", Appl. Phys. Lett., vol. 93, p. 081107 (2008).

13 L. Shterengas, G. Belenky, T. Hosoda, G. Kipshidze, S. Suchalkin, "Continuous wave operation of diode lasers at 3.36 μm at 12 degrees C", Appl. Phys. Lett., vol. 93, p. 011103 (2008).

14 L. Shterengas, G. Belenky, G. Kipshidze, T. Hosoda, "Room temperature operated 3.1 μm type-I GaSb-based diode lasers with 80 mW continuous-wave output power", Appl. Phys. Lett., vol. 92, p. 171111 (2008).

15 T. Hosoda, G. Belenky, L. Shterengas, G. Kipshidze, M. V. Kisin, "Continuous-wave room temperature operated 3.0 μm type I GaSb-based lasers with quinternary AlInGaAsSb barriers", Appl. Phys. Lett., vol. 92, p. 091106 (2008).

16 D. Donetsky, G. Kipshidze, L. Shterengas, T. Hosoda, G. Belenky, "2.3 μm type-I quantum well GaInAsSb/AlGaAsSb/GaSb laser diodes with quasi-CW output power of 1.4 W", Electron. Lett., vol. 43, no. 15, pp. 810-812 (2007).

Book Chapters:

1 G. Belenky, L. Shterengas, M. V. Kisin, T. Hosoda, "GaSb-based Type-I Quantum Well Diode Lasers", Semiconductor lasers: Fundamentals and applications, edited by A Baranov and E Tournie, University of Montpellier, France, Woodhead Publishing Limited, ISBN 0-85709-121-2, ISBN-13: 978 0 85709 121 5, in press.

2 L. Shterengas, G. Kipshidze, T. Hosoda, G. Belenky, "GaSb-based type-I laser diodes operating at 3 μm and beyond", Future Trends in Microelectronics: From Nanophotonics to Sensors and Energy, edited by Serge Luryi, Jimmy Xu, Alexander Zaslavsky, Wiley, ISBN-13: 978-0-470-55137-0, July 2010.

Conference Proceedings:

1 S. Forouhar, C. Frez, K. J. Franz, A. Ksendzov, Y. Qiu, K. A. Soibel, J. Chen, T. Hosoda, G. Kipshidze, L. Shterengas, G. Belenky, “Low power consumption lasers for next generation miniature optical spectrometers for trace gas analysis”, Proceedings SPIE Quantum Sensing and Nanophotonic Devices VIII, vol. 7945, p. 79450M (2011).

2 T. Hosoda, J. Chen, G. Tsvid, D. Westerfeld, R. Liang, G. Kipshidze, L. Shterengas, G. Belenky, "Progress in development of room temperature CW GaSb based diode lasers for 2-3.5 μm spectral region", International Journal of High Speed Electronics and Systems, vol. 20, no. 1, pp. 43-49 (2011).

3 J. Chen, T. Hosoda, G. Tsvid, R. Liang. D. Westerfeld, G. Kipshidze, L. Shterengas, G. Belenky, "Type-I GaSb based diode lasers operating at room temperature in 2 to 3.5 μm spectral region", Proceedings SPIE Laser Technology for Defense and Security VI, vol. 7686, p. 76860S (2010).

4 G. Belenky, D. Donetski, L. Shterengas, T. Hosoda, J. Chen, G. Kipshidze, M. Kisin, D. Westerfeld, "Interband GaSb-based laser diodes for spectral regions of 2.3-2.4 um and 3-3.1 um with improved room-temperature performance", Proceedings SPIE Quantum Sensing and Nanophotonic Devices V, vol. 6900, p. 690004 (2008).

Conference Presentations:

1 G. Tsvid, A. Soibel, T. Hosoda, J. Chen, G. Kipshidze, L. Shterengas, C. F. Frez, S. Forouhar, G. Belenky, "Type-I GaSb based diode single lateral mode lasers operating at room temperature in 3.1-3.2 μm spectral region", Photonics West, January 2011.

2 G. Belenky, L. Shterengas, G. Kipshidze, T. Hosoda, J. Chen, "Advances in the development of type-I quantum well GaSb-based diode lasers", Photonics West, January 2011.

3 S. Forouhar, C. Frez, A. Ksendzov, Y. Qiu, K. J. Franz, A. Soibel, J. Chen, T. Hosoda, G. Kipshidze, L. Shterengas, G. Belenky, "Low power consumption lasers for next generation miniature optical spectrometers for trace gas analysis", Photonics West, January 2011.

4 L. Shterengas, G. Kipshidze, T. Hosoda, G. Tsvid, G. Belenky, "Diode lasers emitting above 3 μm at room temperature with more than hundred of mW of continuous wave output power", Photonics West, January 2010.

5 Gregory Belenky, Gela Kipshidze, Takashi Hosoda, Jianfeng Chen, Ding Wang, Leon Shterengas, "GaSb-based laser operating within the spectra range of 2-3 μm", Advanced Workshop on Frontiers in Electronics (WOFE), December 2009.

6 Takashi Hosoda, Gela Kipshidze, Leon Shterengas, David Westerfeld, Sergei Suchalkin, "3 μm Type-I GaSb-based diode lasers operating at room temperature in CW mode", 26th North American Molecular Beam Epitaxy Conference, August 2009.

7 Gregory Belenky, Leon Shterengas, Gela Kipshidze, Takashi Hosoda, Jianfeng Chen, Sergei Suchalkin, "GaSb-based Laser diodes operating within spectral range of 2-3.5 μm", Conference on Lasers and Electro-Optics (CLEO), May 2009.

8 Gregory Belenky, Gela Kipshidze, Leon Shterengas, Dmitry Donetsky, Takashi Hosoda, Jianfeng Chen, Sergei Suchalkin, "GaSb based lasers operating within spectral range above 2 μm", Photonics West, January 2009.

9 Gregory Belenky, Leon Shterengas, Gela Kipshidze, Takashi Hosoda, Sergei Suchalkin, "Advances in the development of the GaSb-based laser diodes operating within spectral range of 2-3.5 μm", 21st Annual Meeting of the IEEE Lasers and Electro-Optics Society (LEOS), November 2008.

10 Leon Shterengas, Gela Kipshidze, Takashi Hosoda, Dmitry Donetsky, Gregory Belenky, "Room Temperature Operated 3.1-μm Type-I GaSb-based diode lasers with 80 mW continuous wave output power", Conference on Lasers and Electro-Optics (CLEO), May 2008.

11 S.Suchalkin, D.Westerfeld, S. Jung, G.Kipshidze, L.Shterengas, T.Hosoda, G.Belenky, "Room temperature operated GaSb-based type I light-emitting diodes", SPIE Defence and Security, March 2008.

Acknowledgments

This work could not be accomplished without the help of the members of Optoelectronics Group.

I would like to thank Dr. Gela Kipshidze, Dr. Sergey Suchalkin, Professor Dmitri Donetski, and Professor David Westerfeld for their help and friendship over the entire period of work on my dissertation.

I wish to express my special thanks to my advisers, Professor Gregory Belenky and Professor Leon Shterengas for many helpful discussions and guidance.

Chapter 1. Introduction

1.1: Applications of laser diodes in Mid-infrared spectral range

Semiconductor laser is a device that emits amplified coherent light based on the stimulated emission of photons utilizing the energy transition of electrons in semiconductors. First semiconductor laser was invented and implemented at 1962 [1, 2, 3]. Since then semiconductor lasers have been rapidly developing to one of the most important optoelectronics devices and implemented in many areas for varieties of purposes. Some of the advantages of semiconductor lasers are compactness (can be embedded to mobile devices), low power consumption (can be turned on at some mA of current with small circuitry), modulability (can be modulated directly by modulating input signals), mass productivity (available semiconductor fabrication technology), inexpensive production costs and many more. Such versatilities and advantages, which other types of lasers do not possess, have made and will make the semiconductor lasers so popular and useful in many applications. In mid-infrared spectral range especially in 2-4 μm, GaSb-based lasers should be ideal light sources for many applications.

Dentistry is one of the possibilities. Recent dentistry relies more on Er: YAG lasers for pain free dental cares utilizing water absorption line around 3 μm [4, 5]. Including cavity cares, gum diseases and many other treatments can be done without pains. Human teeth consists of water as a major component and water can be evaporated and removed together with surrounding structures by applying the pulsed emission of Er: YAG lasers at 2.94 μm. GaSb-based lasers could replace Er: YAG lasers any time soon. Gas detection or leakage monitoring systems could be another

example. Such system with high accuracy could be realized in this spectral range due to strong characteristic absorption bands of many industrial gases in the spectral range: C_2H_2 (3.067 μm), CH_4 (3.260 μm), HCl (3.396 μm), HBr (3.775 μm) [6, 7]. Some other possible applications include biological spectral analysis, remote explosive identification, medical diagnostic tools, free space transmitters, surgery instruments, infrared countermeasures and light detection and ranging (LIDAR) [8]. It is important to note that the spectral range of 2.7-3.0 μm has strong water absorption lines—good for medical instruments and the range in 3-5 μm provides atmospheric transparency windows with minimum background noises—good for spectroscopic applications.

1.2: Type-I diode laser design and characteristics

Figure 1 shows the diagram of an edge emitting diode laser. From the bottom of the figure, we have n- (p-) metal contact, n- (p-) doped substrate, a graded buffer layer, n- (p-) cladding layer, active region, p- (n-) cladding layer, graded buffer layer, p- (n-) cap, current confinement layer (dielectric layer), and p- (n-) metal contact. Graded buffer layers are inserted to promote carrier injection. The dielectric layer is formed on the grown structure so that the injected current is confined in stripes where the spontaneous and stimulated emission is amplified. Emitted photons are amplified between two cleaved facets and eventually reach the lasing condition by overcoming the internal optical loss and the mirror loss. The facets are either uncoated or coated to have a specific reflectivity. The laser with simple dielectric layer on the top of grown structures is called gain guided (Figure 2a), and the one with ridge structures is called index guided (Figure 2b). Gain guided devices weakly confine the current and some of the

spread current may be considered as lateral current leakage. Meanwhile, index guided devices normally provide defined current paths by means of ridge structures, which may result in lower threshold current due to very small lateral current spreading or leakage.

The energy diagram of a typical type-I diode laser grown on a substrate is shown in Figure 4a (relative energies to vacuum level is shown in Figure 3). Cladding and graded buffer layers are doped to either n- or p- type to promote carrier injection into the active region. Waveguide layers and QWs are generally undoped to reduce the free carrier optical losses. As certain voltage is applied between the n- and p-contacts, carriers start flowing through the structures. Electrons and holes are injected from n- and p- side, respectively (Figure 4b). Both carriers eventually diffuse into QWs, recombine each other, and generate photons. Efficient laser should have QWs with sufficient confinement of both electrons and holes by providing the band offset with waveguide and barrier layers.

Assuming an electron in conduction band and a hole in valence band are recombined with the energy difference of E electron volt (eV), the wavelength of emitted photons λ is given in the equation as follows:

$$\lambda(\mu\mathrm{m}) = \frac{1.24}{E(\mathrm{eV})}$$

QWs have discrete quantum states in the conduction and valence band due to energy quantization. The energy of emitted photons E is the sum of bandgap E_g and the quantized energy level. Quantization energy is higher if a QW is narrower and the band offset with an adjacent barrier layer is higher.

The light-current characteristic of a semiconductor laser is expressed as follows:

$$P_{out} = \eta_i \frac{\alpha_m}{\alpha_i + \alpha_m} \frac{hv}{q}(I - I_{th}) = \eta_i \frac{\alpha_m}{\alpha_i + \alpha_m} \frac{1.24}{\lambda(\mu m)}(I - I_{th}) = \eta_{slope}(I - I_{th})$$

where P_{out}: output power, η_i: internal efficiency, α_m: mirror loss, α_i: internal loss, I: applied current, I_{th}: threshold current, and η_{slope}: slope efficiency. The output power P_{out} increases linearly as a function of applied current I with the coefficient of η_{slope} when applied current I is larger than threshold current I_{th}. The laser performance in a given condition is determined by the slope efficiency η_{slope} and the threshold current I_{th}.

The slope efficiency can be improved by increasing the internal efficiency and reducing the internal loss. The internal efficiency is the ratio of the number of emitted photons to the total number of injected carrier pairs. The injected carriers are generally lost in the heterostructure as lateral leakage, heterobarrier leakage, and recombination loss. The lateral carrier leakage is the carrier spreading outside of the active region (Figure 5), which can be reduced by having ridge structures or buried heterostructures. The heterobarrier leakage is the thermionic emission from waveguides to doped cladding layers (Figure 6) following the expression:

$$I_{HL} \propto T^2 \exp\left(-\frac{\Delta E}{kT}\right)$$

The leakage is the exponential function of the band offset and can be successfully removed by employing the adequate band offset between the layers in both the conduction and valence bands.

Internal loss is another important figure to determine the slope efficiency. Emitted photons are amplified along the stripe or the ridge and between the cleaved facets. In a set of the material system grown on a wafer, a material of a lower bandgap generally have a higher optical refractive index compared to the one of a higher bandgap. It

means that cladding layers have a lower refractive index compared to the waveguide layers and QWs. Figure 7 shows the refractive index profile and the corresponding optical mode intensity for a laser heterostructure. Optical mode intensity is maximized in the middle of the waveguide where QWs are normally located, and the tail of the optical field overlaps with cladding layers. The optical confinement in layer a is defined as

$$\Gamma_a = \frac{\int_{a_1}^{a_2} E^2(y)dy}{\int_{-\infty}^{+\infty} E^2(y)dy}$$

where direction of y is normal to interfaces of layers. Layer a is between the position of a_1 and a_2. The internal loss is expressed as follows:

$$\alpha_i = \Gamma_{clad}\alpha_{clad} + \Gamma_{wg}\alpha_{wg} + \Gamma_{QW}\alpha_{QW}$$

Carrier loss in doped cladding layers α_{clad} is generally larger than the loss in waveguide α_{wg} and QWs α_{QW} due to the contribution of free carrier losses in doped layers. What laser designer can do to reduce internal loss is to increase the waveguide width, to change the composition of the cladding layer, and to reduce the doping levels in cladding layers. First two solutions are to reduce the overlap Γ_{clad} and the third one is to reduce the cladding loss α_{clad}.

The threshold current I_{th} is determined by transparency current I_{tr}, differential gain $\frac{dg}{dI}$, and internal loss α_i as follows:

$$I_{th} = I_{tr} + \frac{\alpha_m + \alpha_i}{\frac{dg}{dI}}$$

The transparency current I_{tr} is the minimal current required to keep the QWs transparent (G=0) at the energy level just above the sum of bandgap and quantization energies. The

transparent carrier density in QWs is determined by the material property of QWs. As discussed above, the amount of current which can be used for the laser emission above threshold current is $\eta_i \times$ injected current. Since the phenomena affecting internal efficiency η_i such as lateral carrier leakage, heterobarrier leakage and recombination losses are effective even below threshold current condition, the transparency current I_{tr} becomes larger as the internal efficiency η_i becomes worse. The modal gain $g = \Gamma_{QW} G$, where G is material gain of the QWs. The material gain G is the predetermined figure by the material property. The differential gain $\frac{dg}{dI}$ could be improved by increasing the confinement factor Γ_{QW} by adjusting the width of the waveguides and/or the material compositions for sufficient refractive indices (detail in chapter 2). The differential gain $\frac{dg}{dI}$ decreases as the internal efficiency η_i deteriorates.

To summarize this section, for the overall laser performance, it is important to have a good internal efficiency η_i, internal optical loss α_i, and QW optical confinement factor Γ_{QW}. The internal efficiency η_i becomes larger by minimizing the carrier leakages, and internal optical loss α_i becomes smaller by attenuating the overlap of the optical field with doped claddings. Both directly affect the laser performances both below and above the threshold current. The QW optical confinement factor Γ_{QW} can be increased to maximize the modal gain g in a given condition.

1.3: GaSb-based Type-I diode laser material systems

Binary, ternary, quaternary, and, recently, quinternary alloys with lattice constants matched or close to the lattice constant of GaSb became increasingly

important materials for mid-infrared optoelectronics. Fundamental band gaps and band alignment of binary arsenides and antimonides define an extraordinary wide range of energies available for band-gap engineering (Figure 8) [9]. Large conduction band discontinuity between AlSb and InAs can be utilized for development of the intersubband quantum cascade lasers for mid-infrared [10, 11, 12]. Staggered band alignment between InAs and GaSb can be utilized to span the spectral range from mid-infrared to far infrared and corresponding optically pumped lasers were reported [13]. Interband cascade lasers were developed using W-QWs in active region [14, 15, 16].

In this section we discuss the peculiarities of the design of diode lasers with type-I QWs in active region. Active type-I QW compositions acceptable for pseudomorphic growth on GaSb substrates restrict the optical range for the corresponding antimonide structures to below 4 μm. The popular choice for cladding and waveguide layers is quasi ternary AlGaAsSb with arsenic composition of less than 8%. With the quasi ternary AlGaAsSb alloy, it is easy to obtain a layer with somewhat wider bandgap while being lattice-matched to GaSb by adjusting the composition of gallium and aluminum with as low as several percent of arsenic. QWs can be grown with quaternary GaInAsSb alloys. The bandgap below 0.41 eV corresponds to the wavelength of 3 μm and above, and such QWs should have indium composition of about 50% and arsenic composition above 20% with 1-2% of compressive strains.

Figure 9 shows the band-edge positions for AlGaAsSb and GaInAsSb alloys lattice matched and 1.5% compressively strained to GaSb as a function of gallium composition. For AlGaAsSb, the band-edge energy of valence band moves down as aluminum composition increases (gallium composition decreases), meanwhile the

energy of conduction band moves up as the aluminum composition increases up to 45% and varies slowly between 45-100%. The combination of the aluminum rich alloy for cladding layers and waveguide and barrier layers with aluminum composition of up to 40% secures more than 200 meV of heterobarries on both conduction and valence band, which should provide negligible amount of heterobarrier leakage.

As indium composition increases in GaInAsSb alloy lattice-matched to GaSb, the band-edge position of both conduction and valence bands moves down. The position of valence band edge could be lower than waveguide (and barrier layers) of the AlGaAsSb alloys and very little hole confinement would be available no matter what composition it is in GaInAsSb QWs. Small valence band discontinuity results in insufficient hole confinement and leads to excessive thermal population of the hole states in the adjacent layers. This keeps the quasi-Fermi level away from the QW valence band edge and increases the threshold carrier concentration. Other than this problem, asymmetry of electron and hole density of states (DOS) in QWs is also the negative factor to deteriorate the laser characteristics. Electron DOS in conduction band is smaller than hole DOS due to anticrossing between the valence subbands [17] inducing strong subband nonparabolicity. The difference in DOS introduces the imbalance of carrier concentrations and quasi-Fermi energy level for lasing states goes deep into conduction band ending up with a higher threshold electron concentration.

Introduction of compressive strain in QWs is the solution for the problems above. Devices with compressive strain of 1% in QWs show the reduction of DOS in valence subbands and balances the electron and hole DOS shown in [18]. It is known that compressive strain splits the first heavy-hole and first light-hole subbands and reduces

hole DOS at the valence band edge. Compressive strain above 1% does not reduce hole DOS anymore, but the energy levels of hole in QWs moves up due to the combined effect of reduced arsenic concentration and increased strain in QWs. As shown in Figure 9, by employing 1.5% of compressive strain in QWs, the band positions of both conduction and valence bands moves up and the hole confinement is supposedly improved with an adjacent AlGaAsSb waveguide and barrier layers.

To improve the hole confinement further, we have employed AlGaInAsSb quinternary waveguide and barrier layers. Adding indium into AlGaAsSb would require more As to satisfy lattice matching to GaSb substrate thus improving hole confinement in GaInAsSb QWs even further. The use of quinternary alloys and beneficial role of compressive strain above 1% in active GaInAsSb QWs will be discussed later in details.

Diode lasers with type-I quantum well (QW) active regions grown by solid source molecular beam epitaxy on GaSb substrates currently operate at room temperature in spectral region from below 2 μm and up to 3.5 μm. Typical laser heterostructure utilizes direct-bandgap GaInAsSb alloys for QWs and AlGa(In)AsSb alloys (with either direct or indirect bandgap) for barriers, waveguide core and cladding layers. Laser active region contains several compressively strained GaInAsSb QWs with the width of the QW layers ranging from 7 to 16 nm. The QW compressive strain in excess of 1% has already become typical in modern laser designs. The total thickness of the laser heterostructure including all auxiliary layers is about 6 μm. Devices operate under forward bias voltage of 1.5 - 2 V. The heterostructure are typically grown onto 2” n-GaSb substrates doped with Tellurium up to 10^{17}-10^{18} cm^{-3}. Recently, 3” diameter epi-ready GaSb substrates became commercially available.

The feasibility of room temperature CW high power operation of diode lasers with emission wavelength above 2 μm was long debatable due to the common belief that the Auger recombination in combination with free carrier absorption should lead to excessive threshold current density for lasing. As of year 2011, however, the room temperature CW operation of GaSb-based diode lasers was achieved at the emission wavelength as high as 3.44 μm. The success in the development of long-wavelength antimonide-based diode lasers can be attributed mainly to a well established fact that the narrowing of the active QW bandgap leads to a reduction of DOS. The electron band-edge effective mass scales down with the material bandgap while the in-plane effective mass in the upper hole subband additionally decreases with the compressive strain. The lower DOS of electrons and holes in lasing states implies lower level of carrier injection required to achieve QW population inversion. Since the optical matrix element does not show pronounced energy dependence in the 1-4 μm spectral range the transparency and threshold carrier concentrations can be expected to scale down with the increasing wavelength.

Hence, it is expected that mid-infrared diode lasers can have much lower transparency and, possibly, lower threshold carrier concentrations as compared to their near-infrared counterparts. Auger recombination is three particle process and its net rate is super linear in carrier concentration. The threshold current density of the mid-infrared diode lasers can be rather low despite plausibly increased probability of the individual Auger event in narrow bandgap QWs.

Detailed calculations of QW optical characteristics show that the increase of the emission wavelength from 2 to 3.5 μm can be accompanied by nearly twofold reduction

of the QW transparency carrier concentration which favorably affects the laser performance. Figure 10 illustrates this trend by showing the concentration dependence of the peak QW material gain (maximum gain of QW confined carriers divided by the QW width) for a set of three 10 nm wide QWs with progressively longer band-edge emission wavelength. All three modeled QW compositions, $Ga_{0.75}In_{0.25}Sb$, $Ga_{0.55}In_{0.45}As_{0.19}Sb_{0.81}$ and $Ga_{0.40}In_{0.60}As_{0.32}Sb_{0.68}$, have been chosen to have the same compressive strain of 1.5% and emit near 1.9, 2.8 and 3.5 μm, respectively. For clarity of presentation, there were chosen the wide-gap $AlAs_{0.08}Sb_{0.92}$ barriers which provide ample confinement for both electrons (from above 600 meV for 1.9 μm to above 1100 meV for 3.5 μm emitting QW) and holes (from above 500 meV for 1.9 μm to above 300 meV for 3.5 μm emitting QW), so that the resulting effect of the reduced QW transparency concentration could be attributed solely to the decrease of the confined carrier DOS. For consistency of calculations all the material parameters for binaries were taken from a single source [9]. Interpolation scheme for alloy materials was adopted from [19], however, the valence band edge bowing was ignored due to the lack of reliable experimental information. Calculations were performed using COMSOL-based simulation software developed at Ostendo Technologies for design of III-V semiconductor optoelectronic components [20]. Special attention was paid to detailed microscopic description of carrier confinement in active QWs. Confined states were calculated using a multi-band matrix Hamiltonian with strain-induced deformation potentials and valence band mixing terms [21]. QW optical characteristics were derived from the calculated complex susceptibility of injected carriers taking into account thermal carrier redistribution between QW subbands. The modeling proved that

transparency concentration improvement in longer-wavelength QWs is predominantly related to the conduction band DOS decrease. Further QW optimization might be necessary to improve the differential gain which remains practically unaffected at transparency level in all three QWs. The QW radiative current at a given concentration decreases with the reduction of the confined carrier DOS thus enhancing the differential gain characteristics with respect to injection current. This effect, however, is more relevant to the performance of shorter wavelength emitters where radiative current constitutes large part of the threshold [22, 23]. In long-wavelength MIR lasers, the radiative component of threshold becomes less important since the radiative recombination rate scales down as a square of the optical transition energy.

To take full advantage of the lower carrier DOS in the narrow-gap active QWs an adequate carrier confinement should be provided in the laser active region. In GaSb-based laser heterostructures the net band offsets between GaInAsSb QWs and Al-containing barriers tend to be distributed unequally between conduction and valence bands. Small valence band discontinuity results in insufficient hole confinement and leads to excessive thermal population of the hole states in the adjacent barriers. This keeps the quasi-Fermi level away from the QW valence band edge and increases the threshold carrier concentration.

As of the year 2011, GaSb-based type-I QW diode lasers demonstrate CW output optical power above 1 W in spectral range 1.9-2.5 μm. Corresponding linear laser arrays produce more than 10 W of CW and 25 W of quasi-CW optical power. These laser diodes demonstrate threshold current densities below 100 A/cm^2 – same if not better than those typical for state-of-the-art GaAs-based diode lasers operating

below 1 μm, i.e. with active QW bandgap above 1.24 eV (Fekete et al., 2008). More than 360 mW of CW output power at a room temperature was reported at 3 μm. These achievements are the result of almost two decades of efforts aimed at technology development and design refinement.

The first room temperature lasing emission in mid-infrared range (2-5 μm) using GaSb substrate was demonstrated under pulsed regime at the wavelength of 2.3 μm with threshold current density of 20 kA/cm^2 [24] and 2.2 μm with 6.9 kA/cm^2 [25]. Both reports employed GaInAsSb/AlGaAsSb double heterostructure (DH) lasers grown on GaSb substrates. The modification in confinement layers was required to reduce the heterobarrier leakage, which in turn was to reduce the threshold current density. The first room temperature CW operation in the spectral range of 2.2-2.4 μm was reported by Bochkarev, et. al. [26]. They increased aluminum content from 35% to 55% in both p- and n-type of AlGaAsSb layers sandwiching GaInAsSb active layer. Meanwhile another group reported $Ga_{0.84}In_{0.16}As_{0.14}Sb_{0.86}/Al_{0.75}Ga_{0.25}As_{0.06}Sb_{0.94}$ DH lasers (λ=2.2 μm) for CW room temperature operation with an improved threshold current density of 940 A/cm^2 in 1991 [27]. The threshold current density was the lowest room-temperature value reported at that time.

The large threshold current density with bulk-like DH lasers was still the biggest bottleneck of the development in the spectral range for CW room temperature operations. At the beginning of 1990s, QW active regions started to be embedded to DH structures providing separate confinement for carriers and photons. The first GaSb-based GaInAsSb/AlGaAsSb QW laser was reported for the operation at the wavelength of 2.1 μm with the threshold current density of 260 A/cm^2 and the maximum CW power

of 190 mW/facet at room temperature [28]. QW lasers operating at 1.9 μm were also reported by the same group [29]. The maximum CW output power was 1.3 W and a pulsed threshold current density was 143 A/cm^2 with strained GaInAsSb/AlGaAsSb QWs. In addition to employing QWs in active region, the design with the broad waveguide separate confinement structure provided lower internal optical losses due to the reduction of free carrier optical losses in doped cladding layers. Garbuzov, et al. reported broad stripe lasers emitting at 2 μm with CW and quasi-CW powers of 1.9 W and 4 W at room temperature, respectively [30]. They inserted 0.4 μm-undoped waveguide layers between doped n- and p-cladding and the strained QWs, successfully reduced the internal optical loss, in turn decreased the threshold current density (115 A/cm^2) and improved the obtainable power at a given injected current density. Modification of aluminum composition in waveguide layer helped to adjust valence band offsets for the adequate hole confinement [31]. The device characteristic temperature T_0 of 140K and differential quantum efficiency of 74% were the big progresses compared to those reported by that time.

The GaSb-based type-I lasers emitting above 2.0 μm were made available by employing both heavily strained QWs and broad waveguide separate confinement layers. Utilizing heavily strained GaInAsSb QWs with improved hole confinement produced diode lasers operating above 2 μm [32, 33, 34, 35, 36, 37, 38, 39, 40, 41]. High power CW room temperature operation was demonstrated with nearly 2.0 W at 2 μm [34], and with more than 1 W within spectral region from 2.3 to 2.5 μm [37, 38]. Improved beam quality was achieved in diode lasers utilizing flared gain section [40, 41].

Single-frequency lasers have been on high demand for spectroscopic applications. Narrow ridge structures were used to fabricate single spatial mode lasers emitting at 2.1 μm [42] and at 2.3 μm [43]. Under certain operating conditions these devices demonstrate single spectral mode operation [43, 44]. Distributed feedback (DFB) lasers with stable single spectral mode operation were developed in the last decade for a range of emission wavelengths: 2.3 μm [45], 2.4 μm [46, 47], 2.6 μm [48], 2.84 μm [49] and 3 μm [50].

Electrically pumped vertical cavity surface emitting lasers (VCSELs) are especially desirable for a variety of the spectroscopic applications and were successfully demonstrated in works [51, 52, 53, 54, 55]. These single mode devices emitting within spectral region from 2 to 2.5 μm are characterized by circular output beam and low energy consumption. The first GaSb-based electrically pumped VCSELs operating near 2.2 μm at 296K in pulsed mode were reported in [51]. CW room temperature operations were reported only after the year 2008 [52, 53, 54, 55]. Low threshold current of the order of several mA were demonstrated for VCSELs with the current and optical confinement achieved by use of buried tunnel junction [52, 55]. Optically pumped vertical external cavity surface emitting lasers were reported emitting in spectral range from 2 to 2.8 μm with nearly diffraction limited output beam and CW power in excess of 1 W [56, 57, 58, 59].

Extensive efforts have been dedicated to development of type-I QW GaSb-based diode lasers operating at wavelength near 3 μm and above. GaInAsSb/AlGaAsSb heterostructures were used in devices operating in CW at room temperature (2.72 μm [60], 2.82 μm [61], 2.96 μm [62], 3.04 μm [63] and 3.1 μm [64]). The lack of valence

band offset between the narrow-bandgap GaInAsSb QWs and AlGaAsSb barrier and waveguide layers was identified as the deficiency of the laser heterostructure [61, 65, 66, 67] that limited an available output power of these devices.

An important step in the development of the long wavelength GaSb-based type-I QW diode lasers was the introduction of quinternary AlGaInAsSb barriers [68, 69, 70, 71, 72, 73, 74, 75]. The use of AlGaInAsSb/GaInAsSb heterostructure in the device active region led to the improvement of the hole confinement in the GaInAsSb QWs. Under pulsed regime, laser operation at the temperatures up to 50 °C was demonstrated at the emission wavelength above 3.3 μm [68]. High power 3 μm lasers based on AlGaInAsSb/GaInAsSb heterostructure demonstrate 360 mW of CW output power at room temperature [74]. CW room temperature operation was achieved above 3.44 μm – the longest wavelength ever reported for GaSb-based type-I diode lasers [73].

Figure 11 shows the reported room temperature operated CW output power of the diode lasers in the wavelength range of 2-3.5 μm (to make the figure more general we incorporate data obtained within period 2008-2011 by efforts described in present work). Until the year of 2004, diode lasers above 3 μm were not available mostly due to the problem of hole confinement. The introduction of quinternary alloys ameliorated the characteristics and made it possible to increase the output power and extend the available wavelength for GaSb-based type-I lasers. Most of the lasers of this type above 3 μm employed the quinternary waveguides and barriers and produced the CW output power of more than 100 mW.

The characteristic temperatures T_0 and T_1 for GaSb-based type-I lasers as a function of emission wavelength in the spectral range of 2-3.5 μm are shown in Figure

12 (we use recent data obtained by us within the period 2008-2011 to make the figure more general). T_0 and T_1 are measured with short pulses with low duty cycle not to increase the device temperature by the injected current. The figures show the exponential temperature sensitivity of threshold current and quantum efficiency, respectively. They keep decreasing as the emission wavelength increases and, above 3 μm, T_0 and T_1 are below 50K and 100K, respectively. The smaller the characteristic temperatures are, the stronger the temperature sensitivity is. As the figures become smaller, devices suffer from degradation of output power due to the high sensitivity to the excessive heat brought by injected current especially under CW regime. Its temperature dependences on the emission wavelength imply several probable phenomena behind the observation. We should identify what are the phenomena to degrade the laser temperature characteristics and then we will understand how to make the lasers operate above 3 μm at room temperature described in the following chapters.

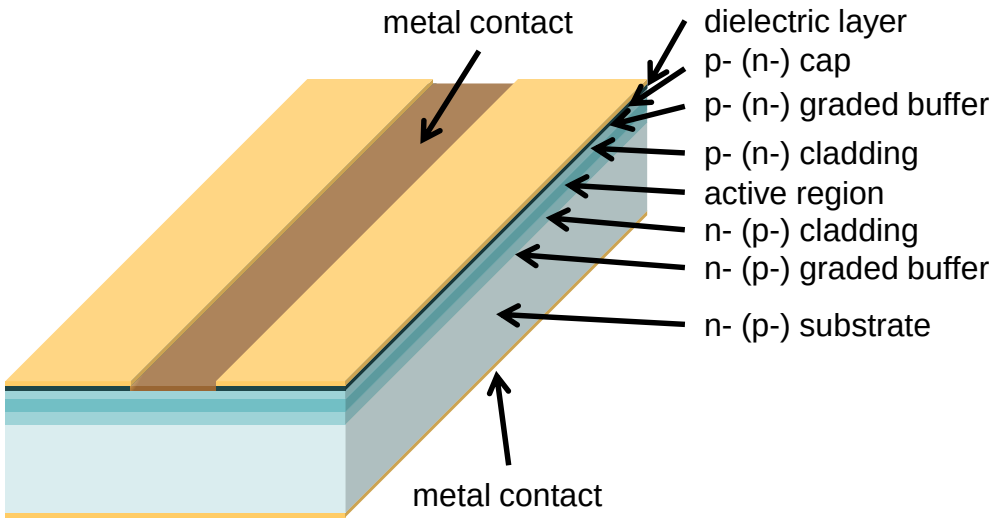

Figure 1: Schematic diagram of an edge emitting laser diode. Graded buffer layers and p- (n-) cap are not shown in the figure.

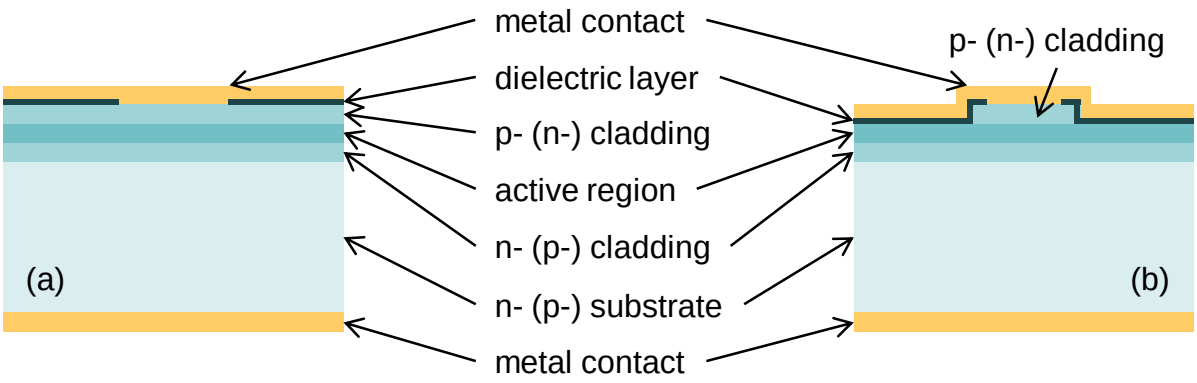

Figure 2: Diagram of a laser facet: (a) gain guided structure, (b) index guided structure.

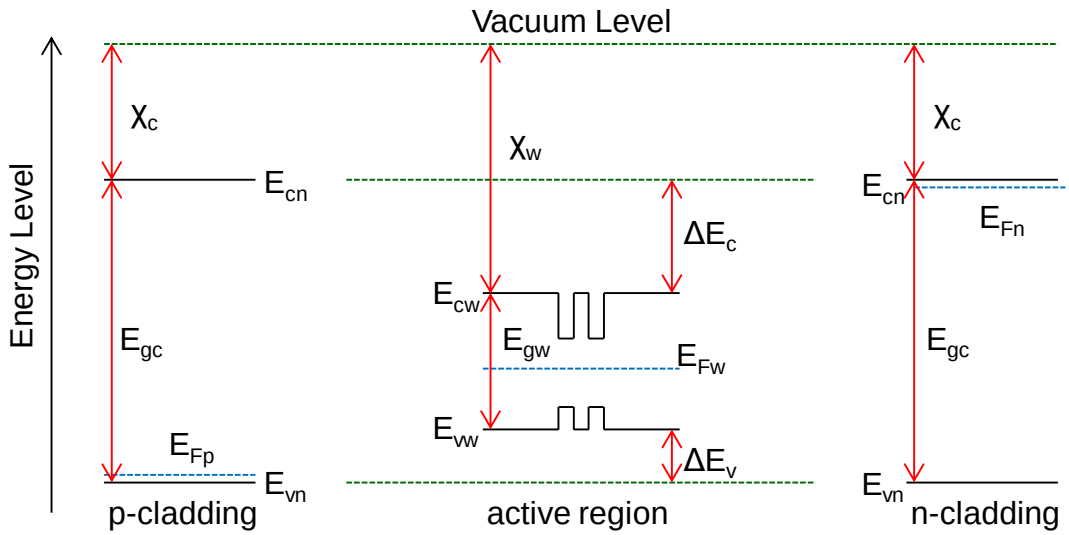

Figure 3: Energy band diagram of materials used in a diode laser. The valence band edge E_v, the conduction band edge E_c, the Fermi level E_F, the vacuum level, the bandgap E_g and the electron affinity X are shown in the figure for each material.

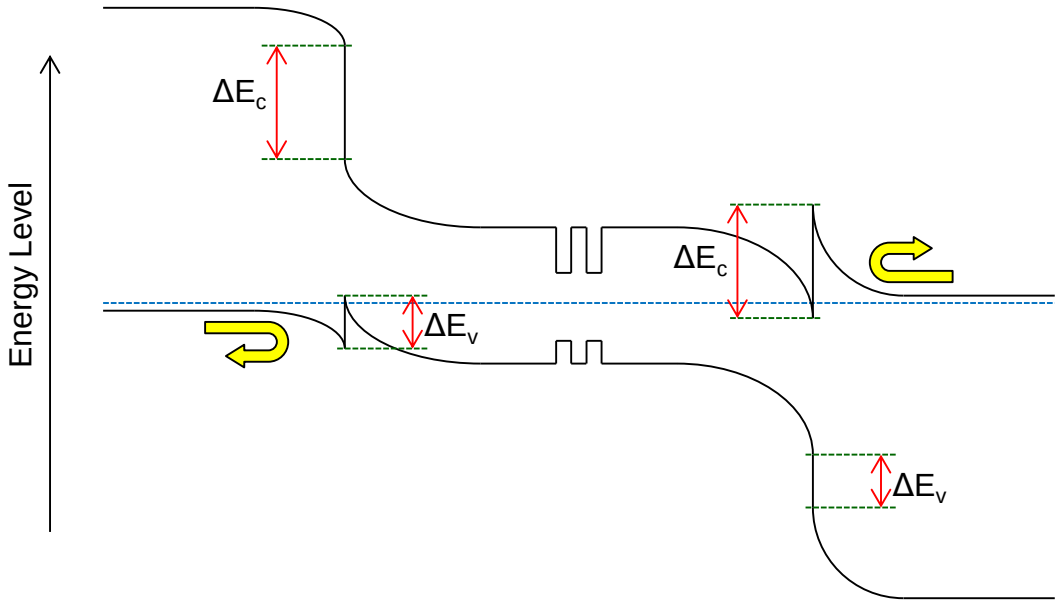

Figure 4a: Energy band diagram of a QW diode laser under equilibrium condition. Blue dashed line indicates Fermi level E_F.

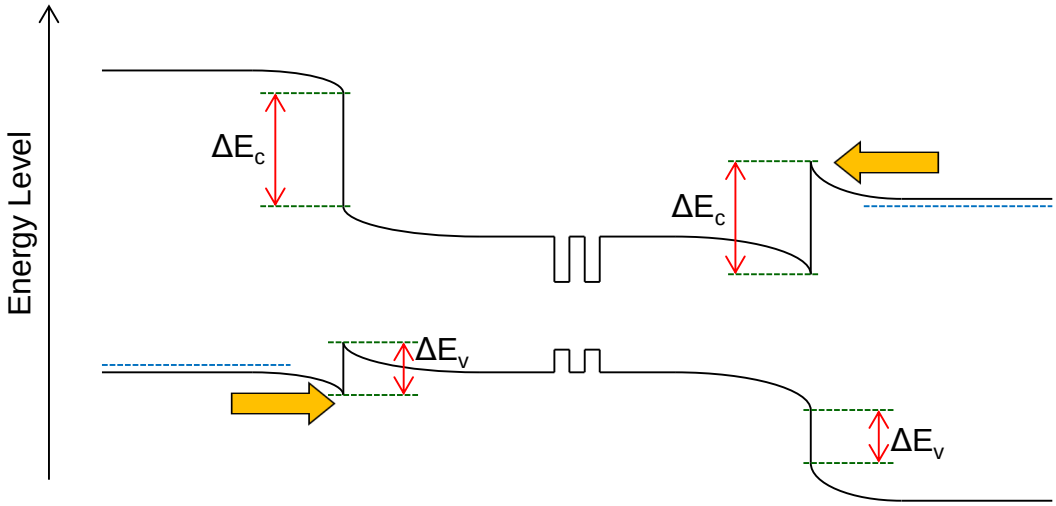

Figure 4b: Energy band diagram of a QW diode laser under forward bias condition. Carriers overcome the energy barriers and flow into QWs.

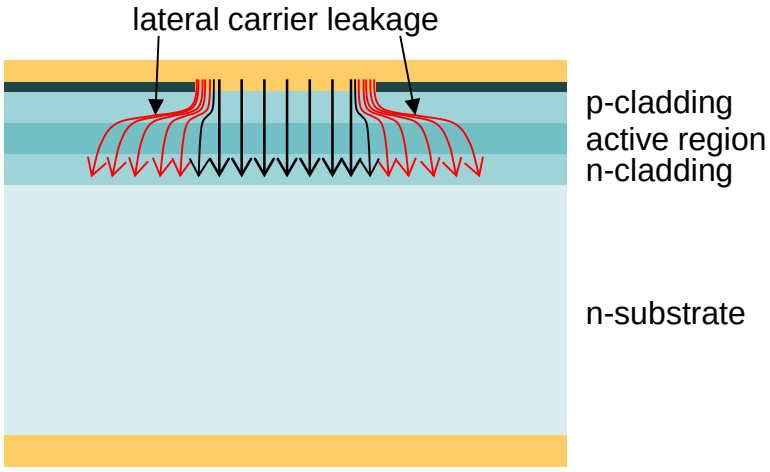

Figure 5: Facet view of a gain guided laser. Red arrows show lateral carrier leakage paths.

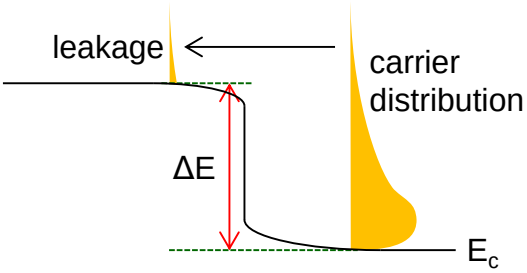

Figure 6: Schematic energy diagram of heterojunction with carrier leakage.

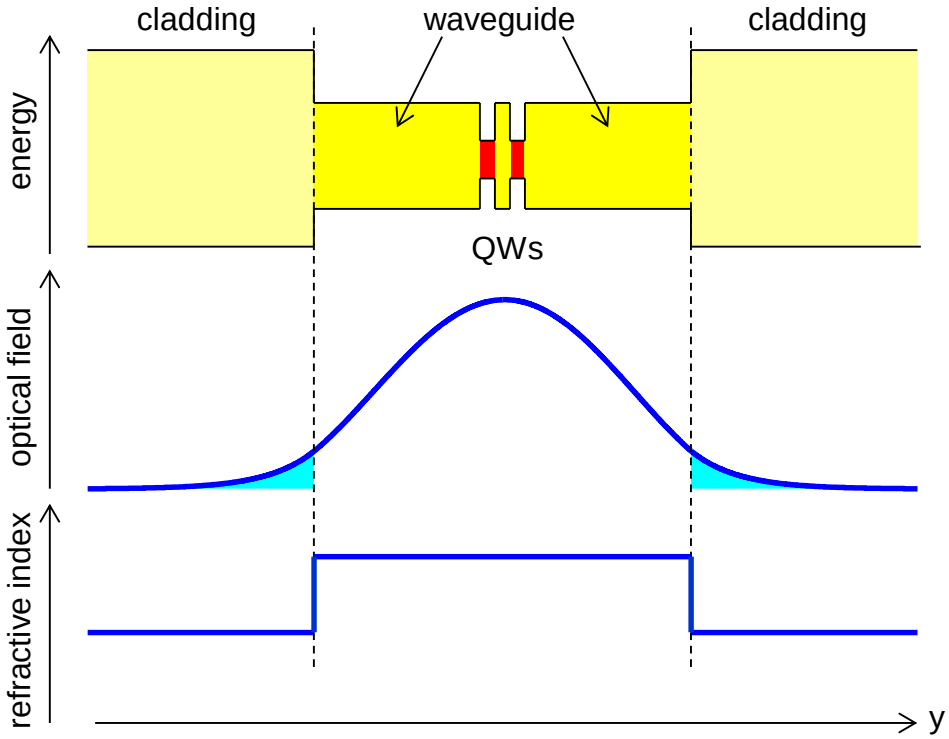

Figure 7: Energy diagram of a laser heterostructure and corresponding refractive index profile and optical field distribution

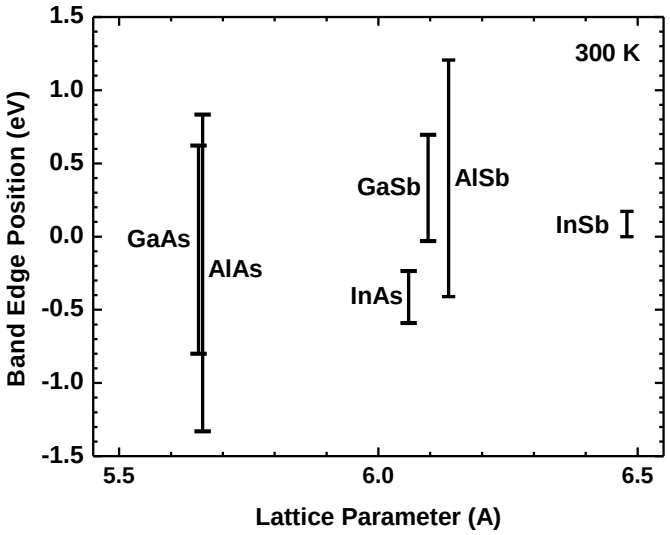

Figure 8: Band gap positions of selected binary alloys. Energy is referenced to InSb valence band top.

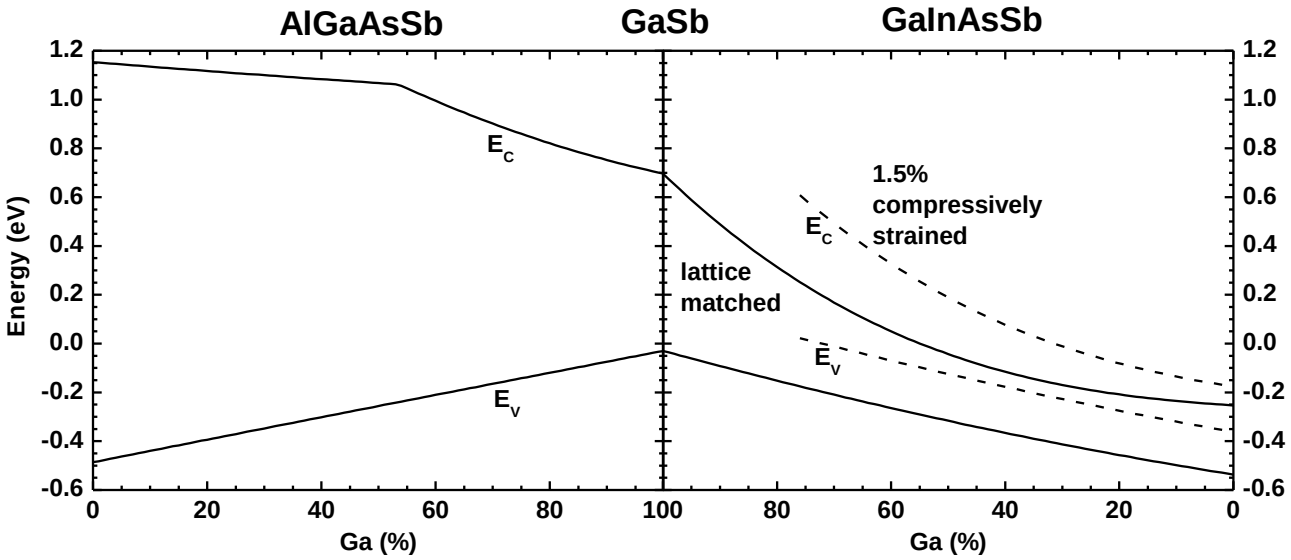

Figure 9: Band-edge positions for AlGaAsSb and GaInAsSb alloys lattice matched to GaSb (solid) and 1.5% compressively strained (dashed). Data according to reference [9]; valence band bowing is neglected.

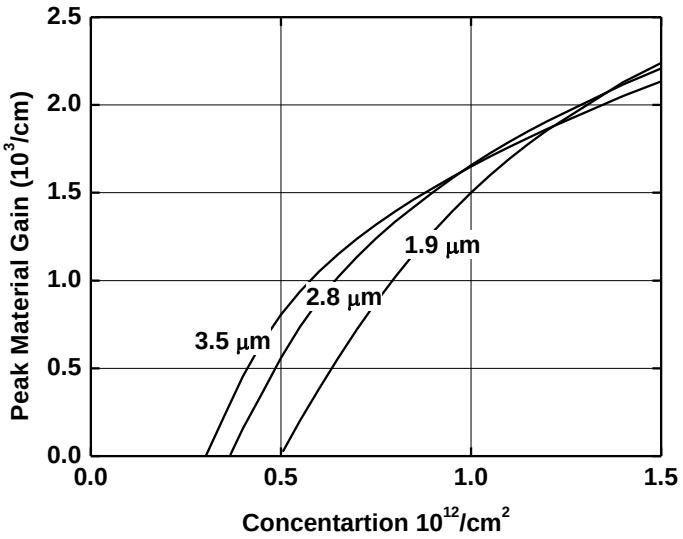

Figure 10: Peak material gain vs. 2D carrier concentration level in three QWs with different emission wavelengths.

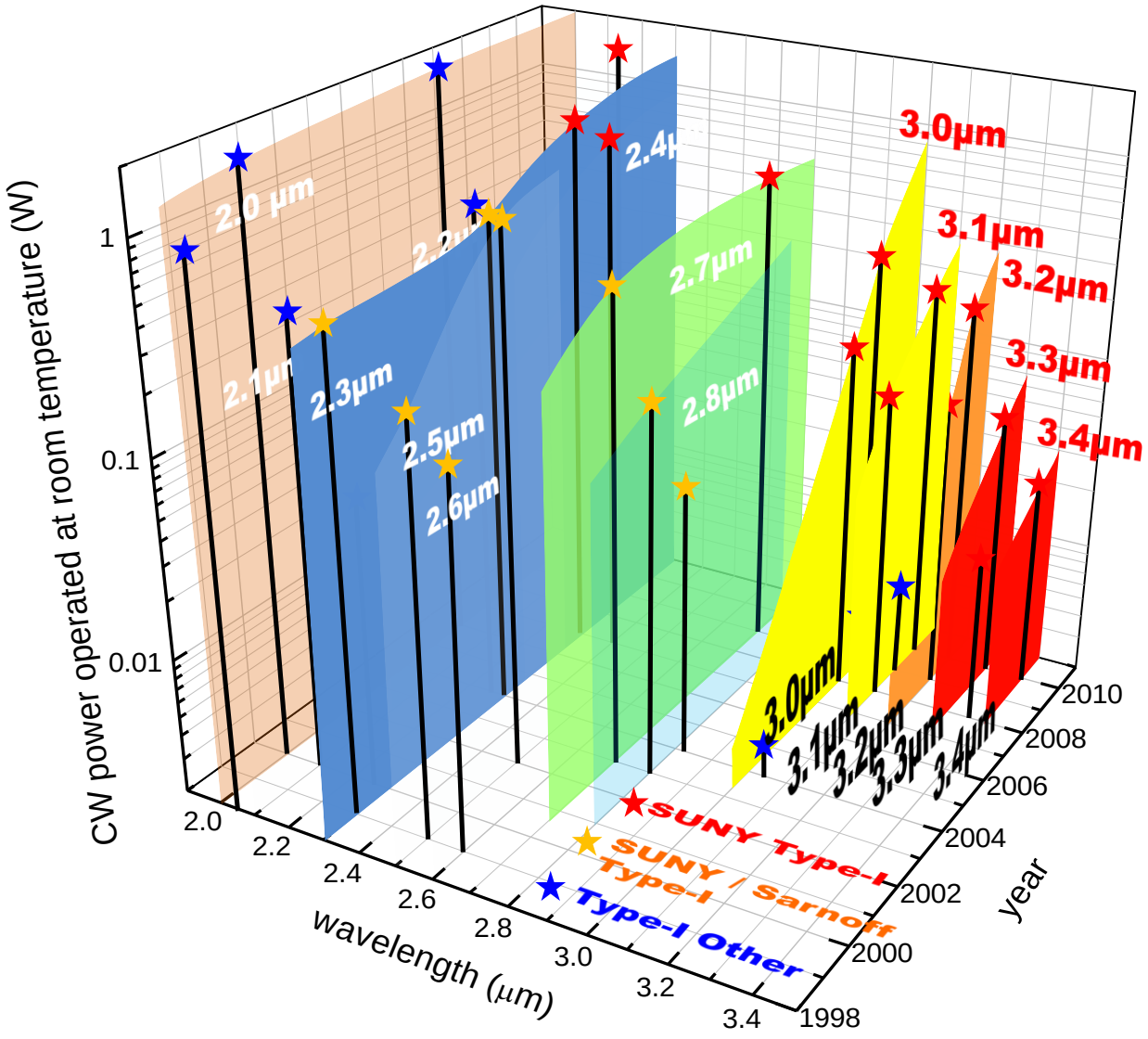

Figure 11: Development of laser diode in the spectral range of 2-3.5 μm (our recent work in the period of 2008-2011 are included).

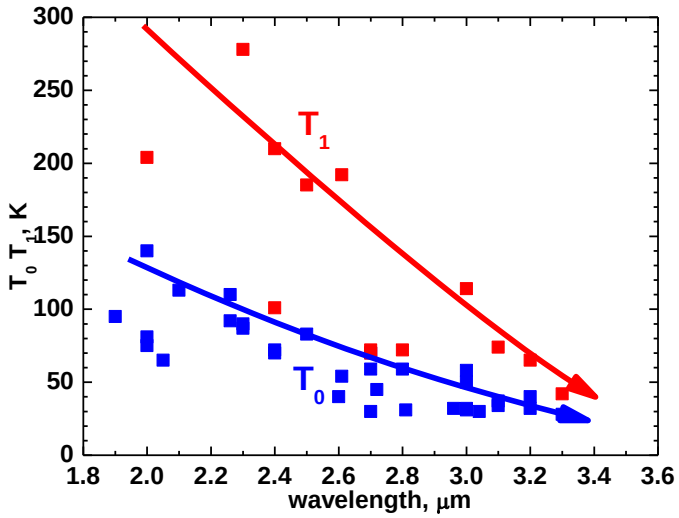

Figure 12: Characteristic temperature T_0 and T_1 for devices in the spectral range of 2-3.5 μm.

Chapter 2. Experimental Results and Discussions

2.1: Introduction

Diode lasers operating in the spectral region above 3 μm are required for a variety of applications. Many important gases and other chemical agents can be remotely detected by tunable laser spectroscopy in this spectral region. For instance, methane, ethane, acetylene, methanethiol, dimethyl sulfide, hydrogen cyanide, etc. absorb strongly between 3 and 4 μm. Analysis of concentrations and isotopic composition of these gasses provides key information on geochemical processes, atmospheric photochemistry, and hydrothermal and biological activity. High power $\lambda \geq 3$ μm beams are required for medical therapy, laser surgery, infrared illumination, countermeasures, etc. Compact, efficient and low cost diode lasers are often preferred components for system realization. High power diode lasers can be used either directly or as pumps for solid state/fiber/nonlinear hosts. In many cases CW operation of diode lasers is either necessary or at least favored. Laser operation at or near room temperature dramatically simplifies the system design. The voltage drop across the diode laser heterostructure is about 1.5 V and is used to achieve the population inversion in the active region and to send current through auxiliary layers.

Composition of GaInAsSb QWs of GaSb-based diode lasers emitting above 3 μm ranges from 50 to 60% of In and from 20 to 30% of As. Mid-infrared diode lasers at wavelengths above 3 μm suffer from temperature sensitivity of both threshold current and external efficiency. Several factors contribute to undesirable temperature sensitivity of the laser parameters. Among them are free carrier absorption and Auger recombination. Besides these fundamental factors there may be heterostructure

deficiencies. They can cause heterobarrier carrier leakage into the cladding, carrier accumulation in the waveguide core and thermal population of useless energy states inside and nearby the active QWs. These deficiencies can be eliminated by improving the material quality and by designing the laser heterostructure with strong carrier confinement.

2.2: Increased aluminum composition in waveguide

A study shows that device room temperature performances of GaSb-based type-I diode lasers degrade as the emission wavelength increases [61]. The cause of the degradation is assumed to be poor hole confinements between AlGaAsSb waveguide/barrier layers and GaInAsSb QWs as the valence band offset decreases due to the compositional change (increase of arsenic) in QWs for higher emission wavelengths. We designed and grew the laser structure having the quaternary waveguide and barrier layers with aluminum content of 35% instead of 25% to improve the QW hole confinement [64].

The lasers operated under CW regime at room temperature as shown in Figure 13. The devices demonstrated threshold current densities of 700 A/cm^2 (350 A/cm^2 per QW) and maximum CW output power was above 80 mW at 12 °C and the injected current of 3.5 A. Voltage across the laser diode at the maximum output power level was less than 1.5 V at room temperature. The devices with same cavity length and facets underwent the measurements of light-current characteristics with short pulse (200 ns / 10 kHz) low duty cycle mode at temperatures in the range of 200-350K (Figure 14). The threshold current increases exponentially with temperature and it becomes nearly 8 A at

350K. The characteristic temperature T_0 is about 50K in the range of 200-300K and 37K in the range above 300K.

This was the first 3.1 μm CW laser based on GaSb-based system operated at room temperature. The combination of waveguides/barrier with quaternary $Al_{0.35}Ga_{0.65}As_{0.03}Sb_{0.97}$ and GaInAsSb QWs of 1.8% compressive strain certainly improved the hole localization in QWs. It contributed to the improvement of the laser slope efficiency and the device differential gain. The reduction of the threshold carrier concentration leads to suppression of the intensity of Auger process.

In the case of GaSb-based type-I diode lasers, in the interface between AlGaAsSb waveguide (barrier) and GaInAsSb QWs provides the confinement barrier offset for electrons more than satisfactory while the valence band offset is much smaller. The deep conduction band discontinuity is introduced at the interface of QWs since the aluminum content in waveguide and barrier layers were increased to 35% (band offset of more than 500 meV for the particular device). Electrons are confined strongly in the deep QWs and they create electrostatic band bending and confine holes in the vicinity of the QWs. This Coulomb attraction may help to provide hole localization near the QWs despite the lack of confinement due to a small valence band offset.

We can note that the high conduction band discontinuity of about 500 meV may lead to carrier heating due to the carrier energy relaxation phenomenon. The increase of carrier temperature in turn leads to reduction of optical gain and carrier delocalization and can be crucial for laser operations. Increased electron and hole threshold carrier concentrations trigger Auger processes which in turn increase the laser threshold current density and temperature sensitivity. When the aluminum content in the barrier

waveguide layer is increased to about 35%, carrier heterobarrier leakage from waveguide to p-cladding becomes possible. The energy position of Γ valley becomes higher and closer to the one of X valley as aluminum content increases. The energies are equal when aluminum content is about 40-50%. The energy position of X valley does not change as a function of aluminum content. The band offset between cladding (aluminum content of about 85-90%) and waveguide will be small enough for electrons to escape to the cladding layer. This process is a strong function of device temperature and may decrease the injection efficiency for the room temperature operation.

The combined effect explained above might have deteriorated the device performances in total as it appeared in the characteristic temperature T_0 as low as 37K in the temperature range beyond 300K. What we have learned in the device is (1) valence band offset between waveguide (barrier) layer and QWs is probably not enough to support good hole confinement, (2) deep conduction band edge discontinuity between them may result in carrier heating leading to poor hole confinement, and (3) carrier heterobarrier leakage into cladding is possible in the waveguide design with $Al_{0.35}Ga_{0.65}As_{0.03}Sb_{0.97}$.

2.3: Quinternary waveguide

Quinternary AlGaInAsSb barrier layers were introduced to provide larger valence band offsets to QWs [68]. Under pulsed regime, the devices demonstrated the operations up to 50 °C at the wavelength of 3.26 μm. Figure 15 illustrates the energy position of valence and conduction band edges for $Ga_xIn_{1-x}AsSb$ alloys lattice matched to GaSb (solid) and 1.5% compressively strained (dashed) (right pane) and $Al_{0.2}Ga_xIn_{0.8-}$

$_x$AsSb (lattice matched to GaSb) (left pane) as a function of gallium content. Band edge positions and energy gaps were calculated based on the data and methods in references [9, 19]. The valence band positions were obtained by linear interpolation. As the indium content increases in quinternary AlGaInAsSb alloy, the energy positions of both the conduction and valence band edge moves down (see Figure 15).

It can be arranged for a conduction band offset to be above 300 meV in GaInAsSb QWs with AlGaInAsSb barriers. Thus in 300 meV deep and 10-15 nm wide QWs with the second subband quantized away by more than 100 meV there is only one electron subband that is populated at room temperature. At the same time the valence band offset can easily become inadequate in GaSb-based material system. The heavy hole subband separation is also small – about 15 meV between the two topmost subbands. Valence band states in the barriers and in the higher order hole subbands can unfavorably increase the number of states available for population in the valence band. One of the critical design tasks is to minimize the number of states in the valence band that are available for population.

The in-plane effective mass in the fundamental heavy hole subband can be reduced nearly to the level of electron effective mass by introducing compressive strain of about 1%. The strain values beyond that range have minor effect on the band-edge heavy-hole density of states, since at such high strain the heavy-hole and light-hole subbands are already well separated in energy. The population of the second heavy hole subband is minimized by the use of relatively narrow QWs. The barrier state population should be minimized by constructing QWs with adequate hole confinement energies.

We employed the $Al_{0.2}Ga_{0.6}In_{0.2}As_{0.24}Sb_{0.76}$ undoped quinternary waveguide (barrier) layers of 500 nm wide sandwiching two QWs from both sides for 3 μm lasers [75]. The two 14-nm-wide $Ga_{0.46}In_{0.54}As_{0.23}Sb_{0.77}$ QWs are separated by the same quinternary barrier of 40-nm wide. The waveguide (barrier) layers and the QWs have the valence band offset of about 160 meV and conduction band offset of about 300 meV. The cladding layers are $Al_{0.6}Ga_{0.4}As_{0.07}Sb_{0.93}$ quaternary material doped with tellurium and beryllium for n-cladding (2.5 μm thick, doped to 1×10^{18} cm^{-3}) and p-cladding (1.5 μm thick, doped to 2×10^{17} cm^{-3} for 0.5 μm adjacent to waveguide and 8×10^{17} cm^{-3} for the rest), respectively. We use 60% aluminum content in the claddings to move down the energy position of conduction band edge. The band offset between the quinternary waveguide and p-claddings with aluminum content of 90% was unnecessarily large to prevent the carrier heterobarrier leakage.

The result of the temperature dependence of CW light-current characteristics is shown in Figure 16. Neutral (~30%) and high-reflection (~95%) (NR/HR) coated 2-mm-long devices demonstrated more than 130 mW CW output power at 290K with threshold current about 0.6 A (300 A/cm^2). Figure 17 shows the light-current characteristics in the temperature range of 240-290K in short pulse low duty cycle regime (200 ns / 10 kHz). The devices demonstrated more than 1 W peak power at the peak current of 12 A without thermal rollover at room temperature, and the device peak power is more than 1 W at 9 A of peak current at 250K. Characteristic temperatures T_0 and T_1 are 58K and 217K, respectively.

Figure 18 shows the modal gain spectra obtained at 290K by Hakki-Paoli method. The cavity length of the device is 0.92-mm long and the facet is uncoated. From the

value of the modal gain in the long-wavelength part of the spectra, where the material gain is zero, the total optical loss is about 26 cm^{-1} and assuming that the mirror loss is about 12 cm^{-1} for 0.92 mm long uncoated devices, the internal optical loss is 14 cm^{-1}.

The internal optical loss of 14 cm^{-1} is higher than those of GaSb-base lasers emitting below 3 μm. The possible reason is that the overlap of optical field with highly doped cladding is increased and so is the free carrier absorption loss. The refractive index of cladding layers increases by changing aluminum content to 60% from 90%. As the difference in refractive indices between claddings and waveguides becomes smaller, the optical field confinement in the active region becomes weaker and decreases the optical confinement factor Γ_{QW}, which is directly proportional to differential gain of the device. The quantum efficiency (~30%) is not as good as those in 2 μm range. We have focused on reducing the internal optical loss and increasing the internal efficiency by changing the composition of cladding layers and the width of waveguide layers discussed in the next section.

Performance of the GaSb-based type-I QW diode laser with wavelength above 2.5 μm was improved once the quinternary AlGaInAsSb alloy was introduced to replace quaternary AlGaAsSb as a barrier material [76]. An increase of the arsenic composition in any of Sb-based alloys tends to lower the position of the valence band on the absolute energy scale. Thus strong hole confinement requirement can be realized by minimizing arsenic composition in GaInAsSb QW and maximizing arsenic composition in AlGaInAsSb barrier materials. This can be realized by maximizing compressive strain in QWs and by maximizing indium and alminum compositions in quinternary barrier materials. Compressively strained QWs require less arsenic and benefit from heavy-

light hole splitting. Quinternary AlGaInAsSb alloys with increased indium and aluminum compositions require more arsenic to maintain lattice matching to GaSb substrate.

2.4: Quinternary waveguide width and role of carrier transport

Our edge emitting lasers confine the generated optical field in the active region to maximize the overlap with the QWs in the middle of active region, where photons are actually generated. The cladding layers sandwiching the active region have to have lower refractive index compared to waveguide layers to confine the optical field. If the difference in refractive index is adequate, optical field is confined well in the active region and the optical confinement factor (Γ_{QW}) is sufficient and overlap of optical field with cladding layers will be minimized. Minimization of this overlap leads to the reduction of internal optical loss due to free carrier loss in doped cladding layers.

To decrease this overlap, the waveguide layer should be wider. While it reduces the internal optical losses related to free carrier absorption in cladding layers, the optical confinement factor (Γ_{QW}) is reduced because the peak of the optical field decreases. The reduction of optical confinement factor (Γ_{QW}) may result in a higher threshold current because the differential gain is reduced correspondingly. We need to find the optimal width of active region for the good laser operation. We employed $Al_{0.2}Ga_{0.6}In_{0.2}As_{0.2}Sb_{0.8}$ quinternary waveguides of variable thickness and two GaInAsSb QWs of 12 nm wide in the middle of the waveguide layer. The claddings consist of $Al_{0.85}Ga_{0.15}As_{0.06}Sb_{0.94}$ quaternary alloys to enhance the optical confinement factor (Γ_{QW}) and to reduce internal optical losses. The detail is as follows [77].

We designed and fabricated three laser heterostructures with different thickness of waveguide layers: (a) 400 nm, (b) 1000 nm, and (c) 1400 nm. The total widths of the layers including waveguides, barriers and QWs for each sample are (a) 470 nm, (b) 1070 nm, and (c) 1470 nm. The claddings are $Al_{0.85}Ga_{0.15}As_{0.06}Sb_{0.94}$ quaternary layer. Aluminum composition was kept about 85% to avoid the rapid oxidation after facet cleaving. Aluminum rich layers are easy to be oxidized, gradually degrade laser performances, and shorten the device lifetime. While 85% and 90% of aluminum in AlGaAsSb layer gives about the same energy position of conduction band edge, 85% of aluminum in the layer reduces the speed of oxidation dramatically [78]. The n-cladding layer is 2.5-μm wide doped with tellurium to the nominal level of 10^{18} cm^{-3} and the p-cladding layer is 1.5-μm wide doped with beryllium to 2×10^{17} cm^{-3} over 500 nm adjacent to waveguide layer, and doped to 8×10^{17} cm^{-3} over the remaining 1 μm. The grown wafers were fabricated to have 100-μm-wide ridge and diced to be 1-mm-long uncoated facets for pulsed measurements and 2-mm-long anti- (~5%) and high-reflection (~95%) (AR/HR) coated facets for measurements of CW light-current characteristics.

Light-current characteristics of the devices (a), (b), and (c) at 290K are shown in Figure 19, the modal gain spectra of devices (a), (b) and (c) in Figure 20, 21, and 22, and the current dependencies of the peak modal gain in Figure 23. Values of slope efficiencies (η_{slope}), internal optical losses (α_i), normalized QW optical confinement factors (Γ_{QW}), differential gains (dg/dI), and internal efficiencies (η_i) are all shown in Table I. The optical confinement factor (Γ_{QW}) is a calculated value from the refractive

indices of waveguides and claddings [79]. The temperature dependence of the CW light-current characteristics for device (a) is presented in Figure 24.

It turns out that devices should have narrower waveguides to achieve lower threshold current and higher output power even by experiencing higher optical losses. At 290K the lasers demonstrated 200 mW optical power and threshold current density of about 200 A/cm^2. Devices with wider waveguides demonstrated stronger roll-over of the CW light-current characteristics and produced about 150 and below 100 mW output power for 1070 (device (b)) and 1470 nm (device (c)) waveguides, respectively.

The internal optical loss gradually decreases as waveguide width increases because the overlap of optical field with heavily-doped cladding layers is reduced in the devices with wider waveguides. The values are 7 cm^{-1}, 5 cm^{-1}, and 3 cm^{-1}, for device (a), (b), and (c), respectively (Table I). Howerever, despite the internal optical loss decreases, the threshold current increases in devices with wider waveguides. The threshold current increases in the order of device (a), (b) and (c) since the effect of the differential gain is stronger than the effect of optical internal losses to determine the threshold current.

Smaller QW optical confinement factor (Γ_{QW}) in wide-ridge devices is one of the reason to lower the differential gain (Table I), but it is not the only phenomenon to degrade the laser performances. The QW optical confinement factor in device (c) is about 66% of the value in device (a), meanwhile the differential gain is only about 37%. It indicates that other factor(s) contributes to deteriorate the differential gain in the devices with wider waveguides.

The internal efficiencies are 68%, 57%, and 45% in devices (a), (b), and (c), respectively (such portions of the injected current reaches QWs and contributes to radiative emission). The only the structural difference among the devices is the width of waveguide. It can be said that, as the width increases, the rate of the carrier reaching QWs decreases. Effects of the carrier transport in the waveguide and the accumulations of carriers in the waveguide region should be the reason for the dependence of the internal efficiency on the width of the waveguide. As injected current increases and passes the threshold condition, the free carrier concentration in waveguides increases without quasi-Fermi energy pinning. The possible effects could be connected with free carrier absorption, induced carrier recombinations in waveguides, heterobarrier leakage from the waveguide to the cladding layers, and the stronger drift carrier transport in broadened waveguide layers.

The free carrier absorption in waveguides would not be a dominant factor deteriorating device characteristics at least vicinity of threshold current (Table I). Figure 25 shows the light-current characteristics of the devices (a), (b), and (c) in short pulse low duty cycle mode (10 kHz / 200 ns) up to 10 A at 17 °C. At higher pumping levels the output power of device (c) with widest waveguides shows the strongest nonthermal saturation. The free carrier accumulation is induced as the injected current increases, and the associated internal optical loss becomes higher under high level of carrier injections. The increase of optical loss leads to the reduction of the slope efficiency due to both free carrier absorption and recombination, and the devices with elongated waveguides are affected more seriously under high level of injection [80]. In any case,

the carrier absorption loss is not the cause of the deterioration of the internal efficiency characteristics near threshold current in the devices with wider waveguides.

The heterobarrier leakage is the thermionic emission overcoming the energy barriers and increases the carrier loss. Taking into account the energies of the barriers at the AlGaAsSb / AlGaInAsSb interface ΔE_C ~ 550 meV and ΔE_V ~ 170 meV [9, 19] one can neglect the role of heterobarrier leakage.

Another possible scenario includes an increased role of drift transport through broadened waveguide layers, hence, increased values of the electric field near QW/barrier interface. The associated band bending can facilitate the thermionic escape of holes from the relatively shallow QWs in the valence band. Our experiment indicates that this scenario is not important. We compare the ratio $\boldsymbol{a = \eta_i^{470} / \eta_i^{1470}}$ with the ratio $\boldsymbol{b = [(dg/dI)^{470} / (dg/dI)^{1470}] / [\Gamma^{470}_{QW} / \Gamma^{1470}_{QW}]}$. The value of ***a*** equal to 1.5 was obtained at currents above threshold. The value of ***b*** depends on the subthreshold gain values and the refractive indices for AlGaAsSb and AlInGaAsSb, and was calculated to be ~1.8. Taking into account the uncertainty of the refractive index for AlInGaAsSb one can conclude that the values of ***a*** and ***b*** are reasonably close.

Therefore, it is reasonable to expect that for near threshold currents (see Figure 19) dependence of internal efficiency on waveguide width $\eta_i(d_w)$ is caused mainly by the effect of carrier recombination in the laser waveguide. At high injection currents optical losses can increase due to the rise of free carrier concentration in the waveguide.

The combined effects of the carrier transport through waveguide and reduction of the QW optical confinement factor did not allow the 3 μm lasers to benefit from associated internal optical loss reduction. This indicates possibility of further device

performance enhancement after detailed material development studies are completed and carrier mobility in quinternary material might be improved.

2.5: Performance characteristics of lasers with different numbers of QWs

We compared the performances of the devices with different number of QWs [81]. We have grown and fabricated the wafers for devices emitting 3.3-3.4 μm with $Ga_{0.46}In_{0.54}AsSb$ QWs. Figure 26 shows the valence and conduction band energies for $Ga_xIn_{1-x}AsSb$ QWs (1.5% compressive strain, shown as dashed line), $Al_{0.2}Ga_xIn_{0.8-x}AsSb$ (lattice matched to GaSb, shown as blue solid line), and $Al_{1-x}Ga_xAsSb$ (lattice matched to GaSb, black solid lines), as a function of gallium content.

We employed undoped quinternary $Al_{0.2}Ga_{0.55}In_{0.25}As_{0.26}Sb_{0.74}$ waveguide (barrier) layers and $Ga_{0.46}In_{0.54}AsSb$ QWs of 1.5% compressive strain (the compositions chosen for heterostructures are indicated as red arrows in Figure 26). To compare the device performances we prepared the devices with two and four QWs. Both have 500-nm-wide waveguides on both sides of 16-nm-wide QWs with barriers of 40- and 20-nm-wide in two-QW and four-QW devices, respectively. The wafers were processed in the exact same manner as the lasers in section 3.2 including the facet coating (NR/HR) and the devices were mounted on Au-coated copper blocks for characterizations.

Figure 27 and 28 shows the CW light-current characteristics of 2-mm-long devices in the temperature range of 200-285K. Output power of four-QW devices is more than 15 mW at 12 °C and at the emission wavelength of 3.36 μm. Meanwhile, two-QW devices have the highest operating temperature of 270K. Four-QW devices are superior near room temperature, but the difference of light-current characteristics becomes smaller between the two types of lasers as temperature decreases, and two-QW devices becomes superior at 200K and below. The temperature dependence of threshold current is stronger in two-QW devices (Figure 29). Two-QW devices have

smaller threshold current below 250K, and four-QW devices have smaller at 250K and above.

To identify the differences between the two types of lasers, current dependences of the modal gain spectra were measured using Hakki-Paoli method. Figure 30 and 31 show the corresponding current dependences of the modal gain spectra of the two-QW and four-QW, respectively, and Figure 32 shows the current dependences of peak modal gain devices at 12 °C. The total optical loss, estimated by the value in the long-wavelength part of the spectra, is 17-18 cm^{-1} for two-QW and 19-20 cm^{-1} for four-QW devices. The total optical loss should be about the same since the structure is exactly same except for the number of QWs (the thickness of total core width including waveguide, barrier and QWs can be said identical). The difference may be from minor inaccuracy of the measurement or in fabrications. The transparency current is 350-400 mA for two-QW devices and 650-700 mA for four-QW devices. Both type of devices have the transparency current of about 180-200 mA per QW.

The reason of differencies in threshold currents stems from the difference in transparency currents as well as in differential gains. The differential gain of two-QW devices decreases as the current increases. Four-QW devices demonstrates a constant differential gain. It implies that radiative recombination rate decreases in two-QW devices due to enhanced Auger recombination and / or hole delocalization from QWs. Auger recombination rate is estimated in proportional to n^3, where n is the carrier concentrations. To see the carrier concentrations in QWs, the width of modal gain spectra is plotted against the peak modal gain in Figure 33. The width of the gain spectra is taken from the energy difference between two transparency levels (one at

bandgap edge and the other at quasi-Fermi level) which is a quasi-Fermi separation of the carriers in QWs. For any given peak modal gain, the spectra width of two-QW devices are much wider than those of four-QW devices. It indicates that two-QW devices require a higher carrier concentration than four-QW devices to achieve the same modal gain. Four-QW devices have less than twice lower current per QW compared to two-QW devices at any point between transparency and threshold, hence those unwanted effects are less pronounced and the differential gain is constant up to threshold current condition.

From the experiments described in this section, it appears that, by adjusting the number of QWs, we can control the intensity of Auger recombination and / or degree of hole localization in QWs. It is particularly important to minimize threshold carrier concentrations for GaSb-based lasers in the spectral range, since Auger recombination rate may be increased and hole delocalization is induced easily due to a smaller band offset as the emission wavelength increases.

2.6: Designs and performances of GaSb-based type-I lasers operating in CW mode at room temperature within spectral range of 3-3.44 μm

Based on the studies discussed in preceding sections, laser heterostructures with heavily compressively strained QWs with quinternary barriers were developed to produce diode lasers operating at room temperature in CW regime in spectral region from 3 to 3.4 μm. The claddings were $Al_{0.85}Ga_{0.15}As_{0.07}Sb_{0.93}$ doped with tellurium and beryllium for n- (2.5-μm thick) and p-cladding (1.5-μm thick), respectively. Doping level of the part of the p-cladding layer adjacent to waveguide was kept around 10^{17} cm^{-3} to

reduce internal losses associated with free hole absorption. Wafers were processed into 100-μm-wide index-guided ridge lasers by wet etching of the top-cladding layer outside of the current stripe. The values of the empirical parameters T_0 and T_1 were measured in pulsed regime near 300K for 1-mm-long uncoated lasers. For CW characterization the coated lasers were indium-soldered epi-side down.

2.6.1: Laser diodes operating at 3.0 μm

Figure 34 shows the CW room temperature light-current and power conversion characteristics of 3 μm emitting lasers. The laser active region comprised two 11-nm-wide 50-nm-spaced GaInAsSb QW with nominal indium composition of 50% and compressive strain of 1.7%. The barrier and waveguide material was $Al_{0.20}Ga_{0.55}In_{0.25}As_{0.24}Sb_{0.76}$ quinternary alloy.

Total width of the waveguide region (from n-cladding to p-cladding) including double-QW active was about 570 nm. Laser mirrors were cleaved and coated for mirror reflectivity of below 5% for anti-reflection (AR) and above 90% for high reflection (HR). The maximum power of 360 mW was achieved at the current of 4.6 A at coolant (water) temperature of 17 °C. The power conversion efficiency was better than 4% for the whole range of operation with maximum value approaching 9% at output power level of about 120 mW. The CW threshold current density was 200 A/cm^2 (100 A/cm^2 per QW). The voltage across laser heterostructure was below 1.4 V at the maximum output power level. Parameters T_0 and T_1 are 50K and 200K, respectively. The current dependence of the modal gain spectra is shown in Figure 35. The internal optical loss of 4-5 cm^{-1} was estimated from longwavelength part of the gain spectrum assuming mirror loss of about 12 cm^{-1}. The transparency current density is below 100 A/cm^2.

2.6.2: Laser diodes operating at 3.1 μm

Figure 36 shows the CW room temperature light-current and power conversion characteristics of 3.1 μm emitting lasers. The laser active region comprised three 13-nm-wide 1.6% compressively strained GaInAsSb QWs separated by 50 nm wide barriers. Quinternary $Al_{0.20}Ga_{0.55}In_{0.25}As_{0.24}Sb_{0.76}$ was used in barriers and waveguide. The nominal indium composition of QWs was more than 50%. The total undoped waveguide core width was about 650 nm from p-cladding to n-cladding.

The maximum CW output power of 190 mW was achieved at the current of 3.8 A at the coolant (water) temperature of 17 °C. The power conversion efficiency was better than 2% for the whole range of operation with maximum value of more than 4% at output power level of about 100 mW. The CW threshold current density was 350 A/cm^2 (about 120 A/cm^2 per QW). The internal loss is estimated to be about 8 cm^{-1} (Figure 37). The devices operated in the spectral region from 3.1 to 3.2 μm at the temperature above 45 °C in CW mode (Figure 38). The values of the parameters T_0 and T_1 are 34K and 74K, respectively.

The strain and composition of the QWs used for 3.1-μm laser fabrication in current work and in Reference 64 are similar but the barriers and waveguide were fabricated from $Al_{0.35}Ga_{0.65}As_{0.03}Sb_{0.97}$ quaternary alloys. The presence of indium in quinternary alloy strongly decreases the energy positions of both conduction band and valence band. This decrease favorably balances the confinement conditions for both electrons and holes improving confinement of holes. We can speculate that this improvement is instrumental for increasing CW output power of 3.1-μm laser to 190 mW.

Figure 39 illustrates the benefits of using quinternary AlGaInAsSb barriers in 3.1 μm lasers. Replacement of the quaternary $Al_{0.35}Ga_{0.65}As_{0.03}Sb_{0.97}$ with quinternary

$Al_{0.2}Ga_{0.55}In_{0.25}As_{0.24}Sb_{0.76}$ barrier alloy improves the hole confinement by about 100 meV (Figure 39a) and leads to twofold decrease of room temperature threshold current density (Figure 39b). Again, at low temperatures the difference tends to disappear since hole confinement offered by both types of barriers becomes equally adequate.

2.6.3: Laser diodes operating at 3.2 μm

Figure 40 shows the CW room temperature light-current and power conversion characteristics of 3.2 μm emitting lasers. The active layer consists of three 13-nm-wide GaInAsSb compressively-strained QWs (1.6%) separated by 50-nm-wide barriers. The nominal indium composition of QWs was near 55%. The total width of undoped waveguide core was about 650 nm from p-cladding to n-cladding. The maximum power of 165 mW was achieved at the current of 4.2 A at the temperature of 17 °C. The CW threshold current density was less than 400 A/cm^2 (about 130 A/cm^2 per QW). The voltage across laser heterostructure was below 1.5 V at the maximum output power level. The internal optical loss is estimated to be about 9 cm^{-1} from Figure 41.

Quinternary $Al_{0.22}Ga_{0.46}In_{0.32}As_{0.30}Sb_{0.70}$ was used in barriers and waveguide. The increase of indium content in the barriers from 25% to 32% increases the valence band offset between QWs and the barriers. The experiment showed that 32% of indium in quinternary AlGaInAsSb barrier improves the characteristics of 3.2 μm emitting lasers. The variation in hole confinement can be considered a primary cause for the difference in performance of 3.2-μm lasers fabricated with different compositions of AlGaInAsSb waveguide. We believe that increased valence band offset between the well and the barrier in the device with 32% of indium composition is responsible for improvement of device parameters. This offset is about 50 meV higher for the improved device with 32%

of indium than for the device with 25%. The results of measurements presented in Figure 42 show that differential gain is higher for devices with elevated band offset between the well and the barrier. The devices emitting in spectral region from 3.2 to 3.3 μm and with adequate hole confinement operated in CW above 40 °C (Figure 43).

From the design point of view, an increase in indium content in the barrier from 25% to 32% leads to the rise of valence band offset between the well and the barrier as well as the decrease of the corresponding offsets between waveguides and cladding layers. Thus the heterobarrier hole leakage from $Al_{0.22}Ga_{0.46}In_{0.32}As_{0.3}Sb_{0.7}$ waveguide into n-cladding would becomes possible. Experiments presented in this work demonstrate that 32% of indium in AlGaInAsSb barrier can be used for further device development.

2.6.4: Laser diodes operating at 3.3 μm

The nominally undoped $Al_{0.20}Ga_{0.55}In_{0.25}As_{0.24}Sb_{0.76}$ waveguide layer with the total thickness of about 650 nm contained three 13-nm-wide strained GaInAsSb QWs (1.6%) centered in the waveguide and spaced 50 nm apart by barriers with the same composition as the waveguide. The nominal indium composition of QWs was above 55%.

The maximum power of 53 mW was achieved at the current of 2.7 A at the coolant (water) temperature of 17 °C (Figure 44). The CW threshold current density was 545 A/cm^2 (about 180 A/cm^2 per QW). The voltage drop across laser heterostructure was below 2 V at the maximum output power level. The internal loss is estimated to be about 9 cm^{-1} from Figure 45. Use of 32% indium content in barriers for 3.3-μm emitters is expected to improve their output power similarly to 3.2-μm devices.

2.6.5: Laser diodes operating at 3.4 μm

Figure 46 shows the CW room temperature light-current and power conversion characteristics of 3.4 μm emitting lasers. The active region consisted of three 13-nm-wide 1.5% compressively-strained $Ga_{0.43}In_{0.57}As_{0.29}Sb_{0.71}$ QWs separated by 50-nm-wide $Al_{0.22}Ga_{0.46}In_{0.32}As_{0.30}Sb_{0.70}$ barrier layers. Waveguide core was formed by the barrier alloy of 250 nm wide on both sides of active region. More than 40 mW of CW output power was obtained at 12 °C. Increase of the heatsink temperature to 27 °C led to twofold increase of the threshold current. Voltage drop across laser heterostructure was below 1.5 V at the maximum output power level. More than 5 mW of CW output power was available at 27 °C with wavelength near 3.44 μm.

Figure 47 shows the modal gain spectra measured at 17 °C by the Hakki-Paoli method for 1 mm-long uncoated lasers. The internal loss is estimated to be about 9 cm^{-1}. This value is essentially the same as the one for broadened waveguide 3.36 μm devices [81] despite the threefold increase of the overlap of the optical field with doped p-cladding. The reason is a twofold reduction of the p-cladding doping layer and a plausible overall decrease of the threshold carrier concentration owing to improved hole confinement. Indeed, Figure 48, which plots the rate of increase of the peak modal gain with current, shows the reduced transparency carrier concentration per QW, i.e. 40 against 60 A/cm^2. Also, no reduction of the differential gain was observed in optimized devices (shown in red) though it was noticeable in a previous iteration of the design (shown in blue) [80].

Increase of the laser wavelength from 3 to 3.4 μm was accompanied by threefold increase of the threshold current density and corresponding reduction of the device

efficiency. It is hardly feasible that probability of individual Auger recombination events could increase threefold when bandgap is reduced by only about 10%. However, to reduce the active region bandgap by 10% the GaInAsSb QWs of 3.4 μm lasers were made wider and incorporated more Indium than QWs of 3 μm lasers. Extra indium requires extra arsenic to maintain pseudomorphic growth. Increased arsenic concentration moves down QW valence band edge on the absolute energy scale thus degrading the hole confinement. Figure 49 illustrates this trend by plotting the compositional dependence of the band edge positions of the GaInAsSb alloy with 1.5% compressive strain.

Increase of QW Indium contents from about 25% (2.2 μm room temperature emission wavelength in 10-15 nm wide QWs) to about 60% (3.5-4 μm room temperature emission wavelength) lowers the QW valence band edge by about 200 meV. Unless barrier material is correspondingly adjusted, the hole confinement will degrade and can even completely disappear. Poor hole confinement increases the number of states in valence band available for thermal population thus increasing threshold carrier concentration and triggering the Auger and other temperature-activated processes that are detrimental to high power room temperature operation of diode lasers.

Table I. Characteristic data of three lasers (a), (b), and (c) with different widths of waveguide. QW optical confinements are normalized to their value for waveguide width of 1470nm (reference [77]).

Samples	d_w [nm]	η_{slope} [W/A]	α_i [cm^{-1}]	Γ_{QW}	dg/dI [cm^{-1}/A]	η_{int} [%]
(a)	470	0.177	7	1.50	113	68
(b)	1070	0.166	5	1.21	84	57
(c)	1470	0.149	3	1.00	42	45

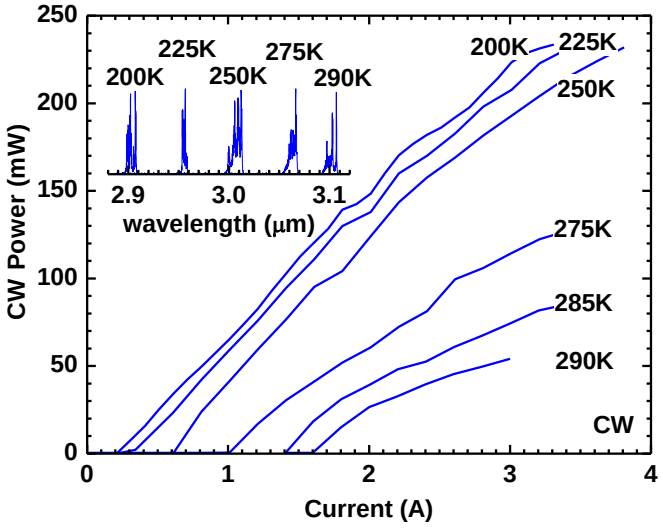

Figure 13: CW light-current characteristics measured in temperature range from 200 to 290K for 2 mm long, 100 μm wide NR/HR (neutral-/high-reflection) coated lasers. The inset shows the laser spectrum near threshold at different temperatures (reference [64]).

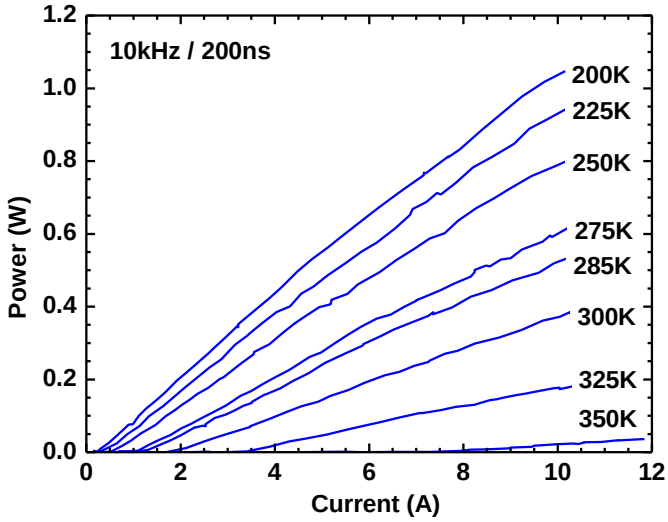

Figure 14: Pulsed light-current characteristics measured in temperature range from 200 to 350K for 2 mm long, 100 μm wide NR/HR coated lasers (reference [64]).

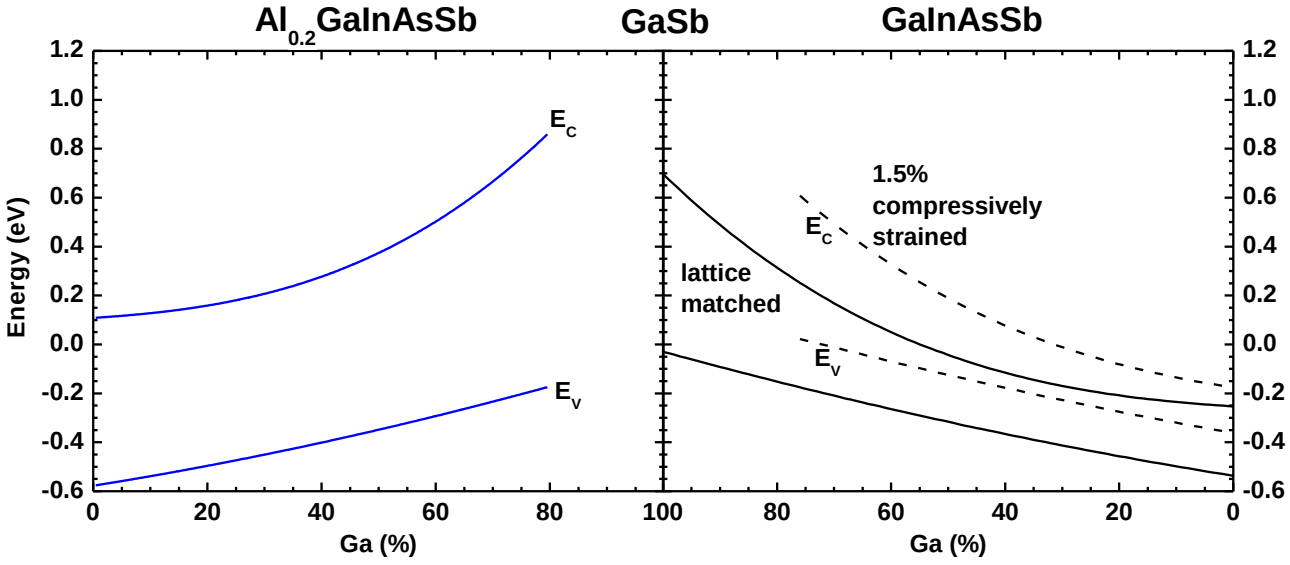

Figure 15: Band-edge positions for $Al_{0.2}Ga_xIn_{0.8-x}AsSb$ and $Ga_xIn_{1-x}AsSb$ alloys lattice matched to GaSb (solid) and 1.5% compressively strained (dashed). Data according to reference [9]; valence band bowing is neglected.

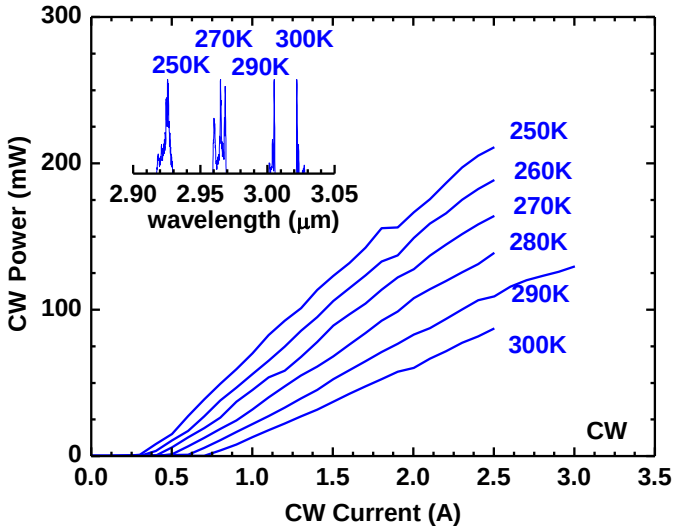

Figure 16: CW mode output power and spectral characteristics of 2-mm-long NR/HR coated device with stripe width 100 μm (reference [75]).

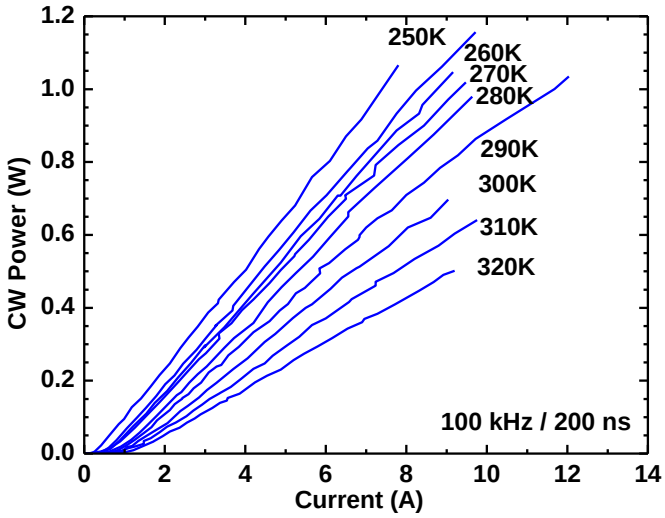

Figure 17: Pulse mode (200 ns / 10 kHz) output power characteristics (reference [75]).

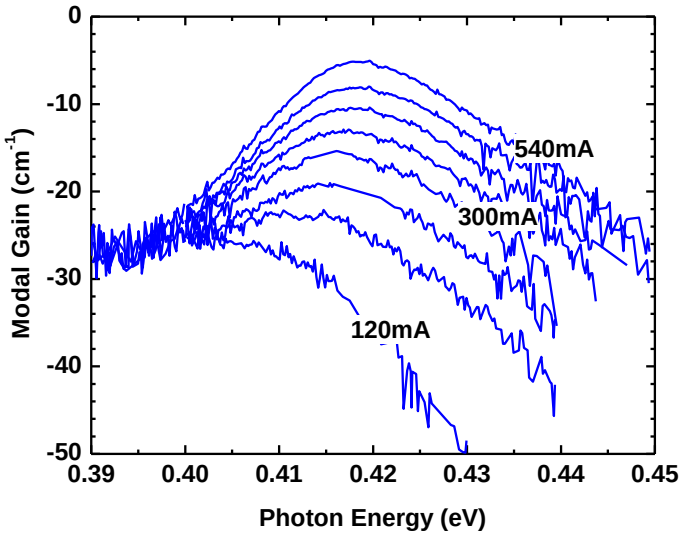

Figure 18: Current dependence of the modal gain of 0.92-mm-long uncoated device at 290K measured in pulse mode (200 ns / 2 MHz) (reference [75]).

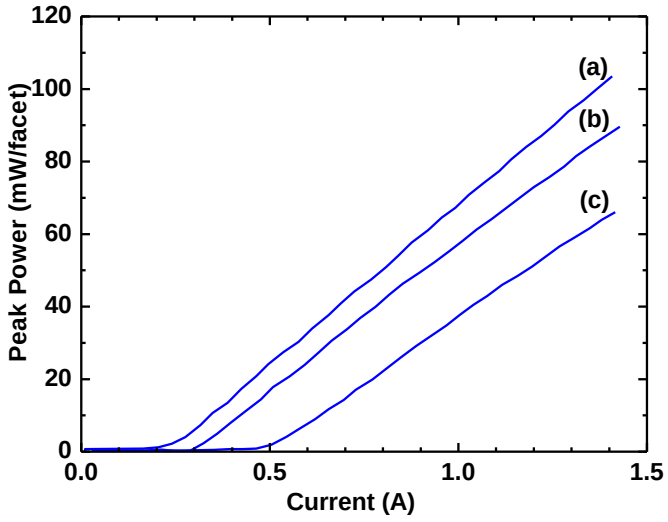

Figure 19: Output light-current characteristics of samples (a), (b), and (c) of 1-mm-long uncoated devices measured under pulsed mode (100 kHz / 200 ns) at room temperature (reference [77]).

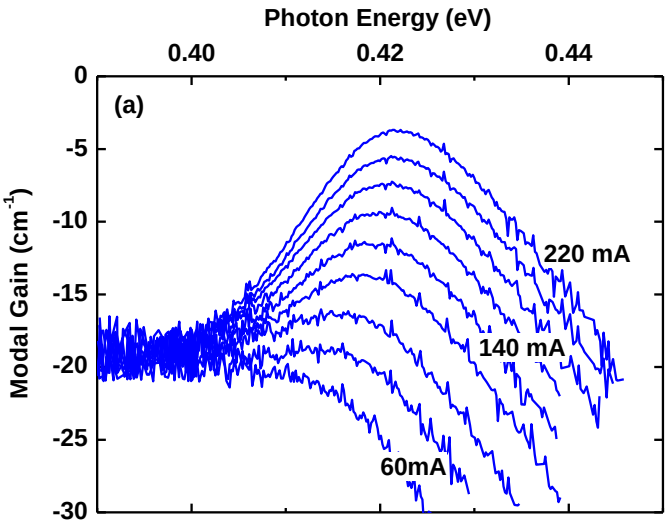

Figure 20: Current dependence of the modal gain spectra of 1-mm-long uncoated device (a) at 290K measured in pulse mode (200 ns / 2 MHz) (reference [77]).

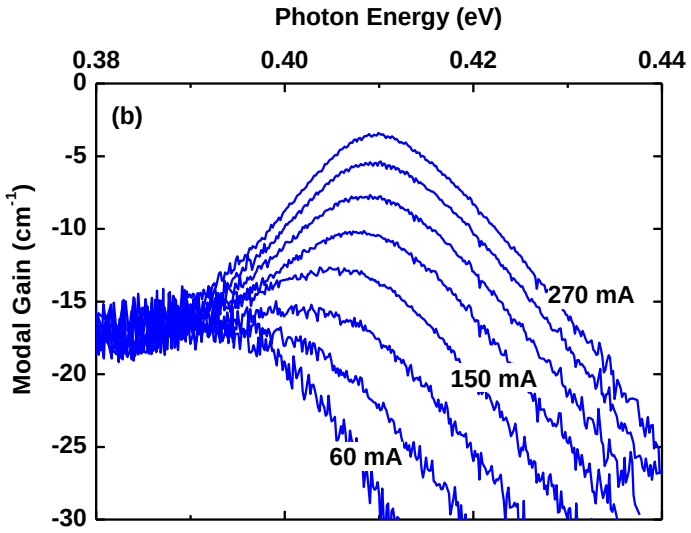

Figure 21: Current dependence of the modal gain spectra of 1-mm-long uncoated device (b) at 290K measured in pulse mode (200 ns / 2 MHz). (reference [77])

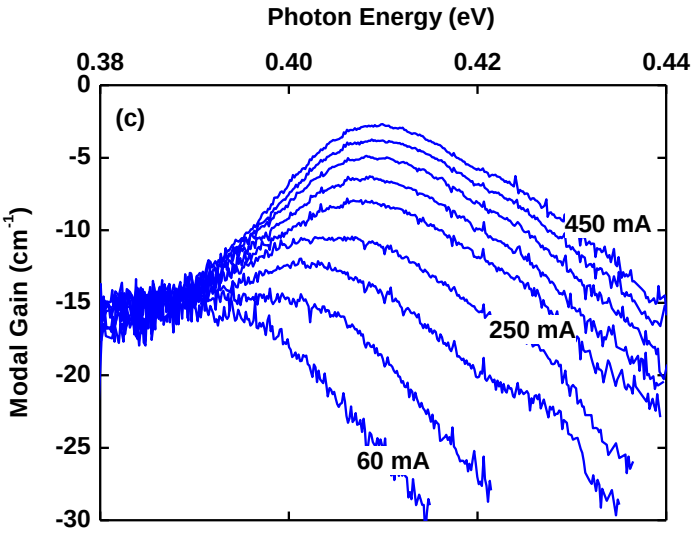

Figure 22: Current dependence of the modal gain spectra of 1-mm-long uncoated device (c) at 290K measured in pulse mode (200 ns / 2 MHz) (reference [77]).

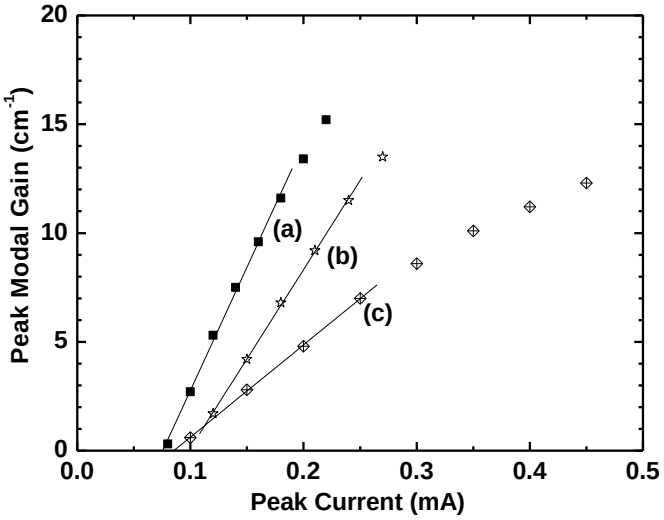

Figure 23: Current dependence of the peak modal gain at room temperature (290 K) of the 1-mm-long uncoated devices with variable waveguide widths (reference [77]).

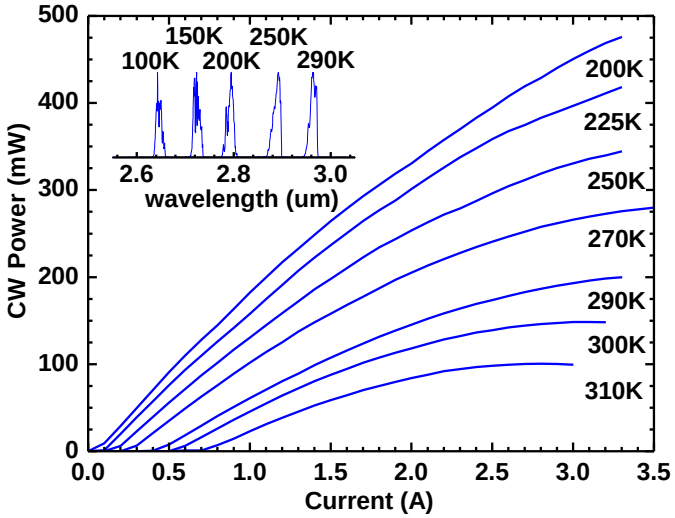

Figure 24: Temperature dependence of cw mode output light-current characteristics of device (a) with 2-mm-long AR/HR coated laser. Inset shows the laser spectra near threshold current at variable temperature (reference [77]).

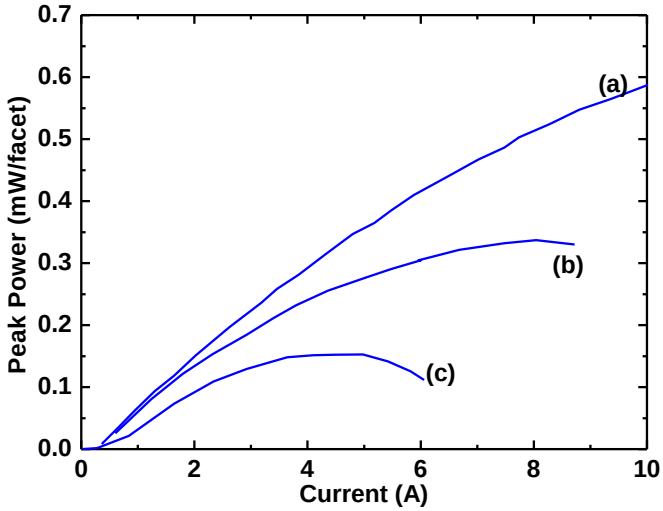

Figure 25: Output light-current characteristics of devices (a), (b), and (c) of 1-mm-long uncoated devices in short pulse low duty cycle mode (10 kHz / 200 ns) up to 10 A at room temperature (reference [77]).

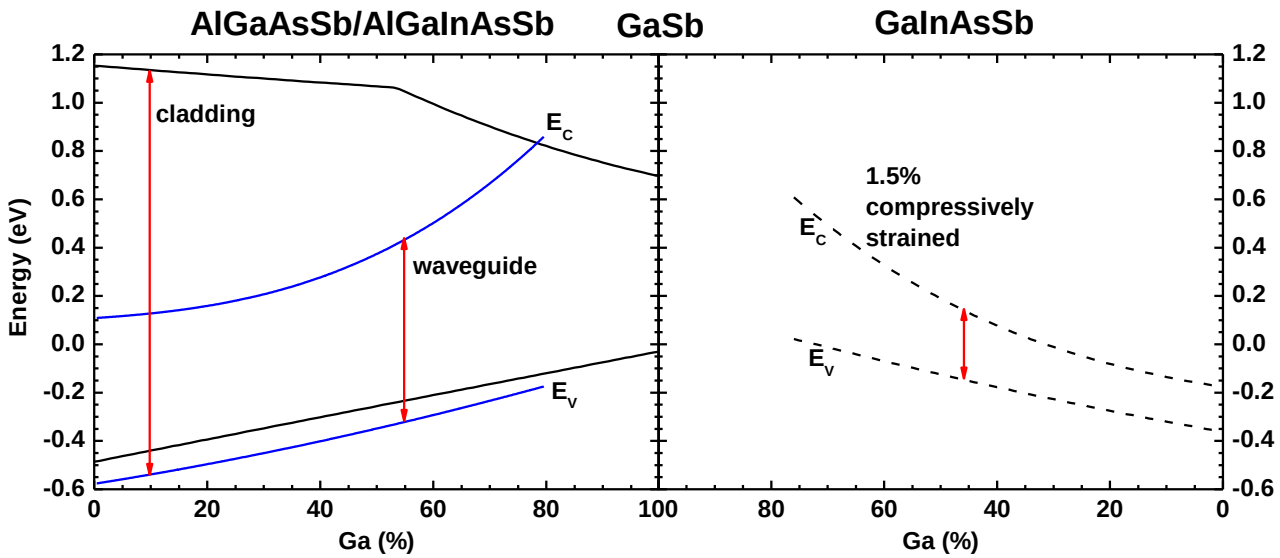

Fgure 26: Conduction and valence band energy positions vs galium concentration for $Al_{1-x}Ga_xAsSb$ (black solid lines) and $Al_{0.2}Ga_xIn_{0.8-x}AsSb$ (blue solid lines) lattice matched to GaSb and 1.5% strained GaInAsSb quaternary QW composition (dashed lines). Red arrows indicate the choice of the materials for the diode laser emitting 3.36 μm.

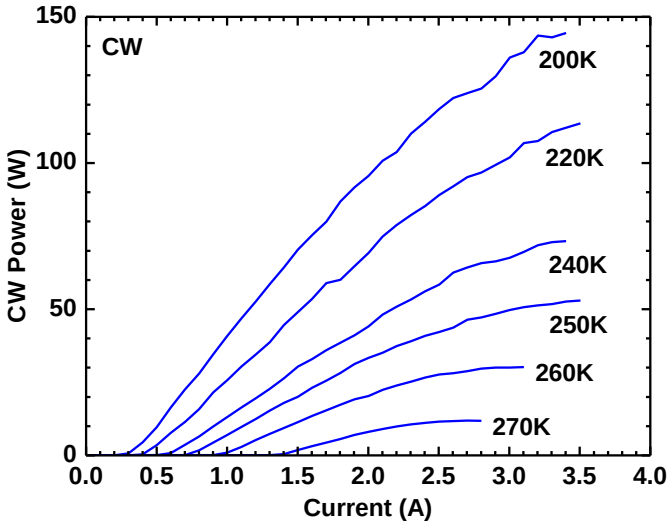

Figure 27: CW light-current characteristics of 3.36-μm 2-QW devices measured in temperature range of 200-285K (2-mm-long, 100-μm-wide lasers) (reference [81]).

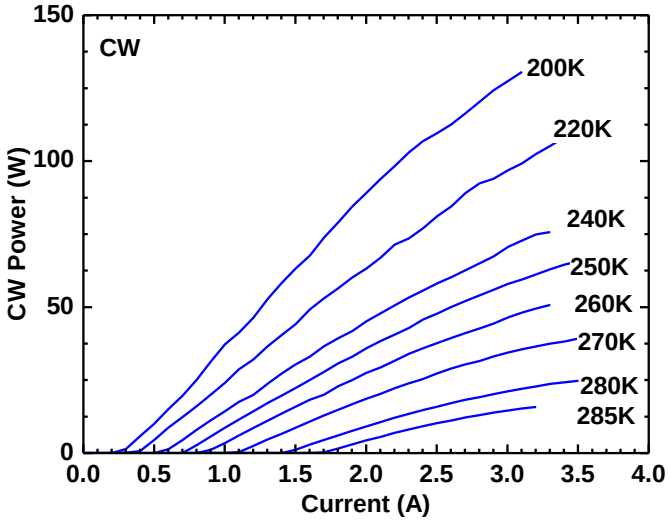

Figure 28: CW light-current characteristics of 3.36-μm 4-QW devices measured in temperature range of 200-285K (2-mm-long, 100-μm-wide lasers) (reference [81]).

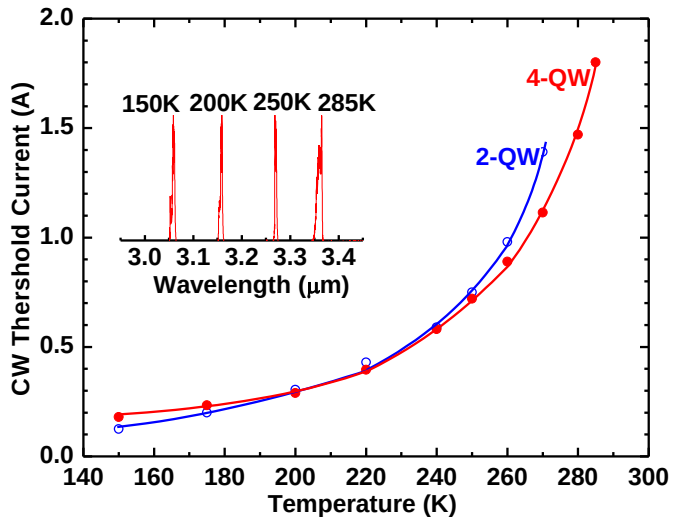

Figure 29: Temperature dependence of CW threshold current of 3.36-μm devices with two QWs and four QWs (reference [81]).

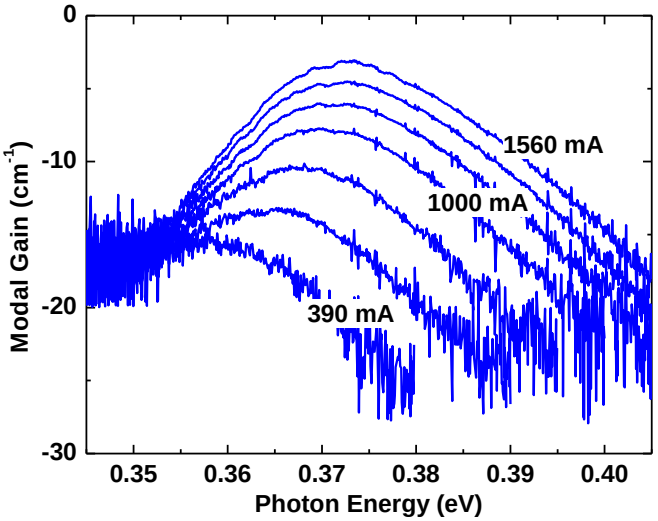

Figure 30: Current dependence of the modal gain spectra measured in pulse mode at (200 ns / 2 MHz) 290K for 2-QW, 1-mm-long, 100-μm-wide, uncoated lasers emitting 3.36 μm.

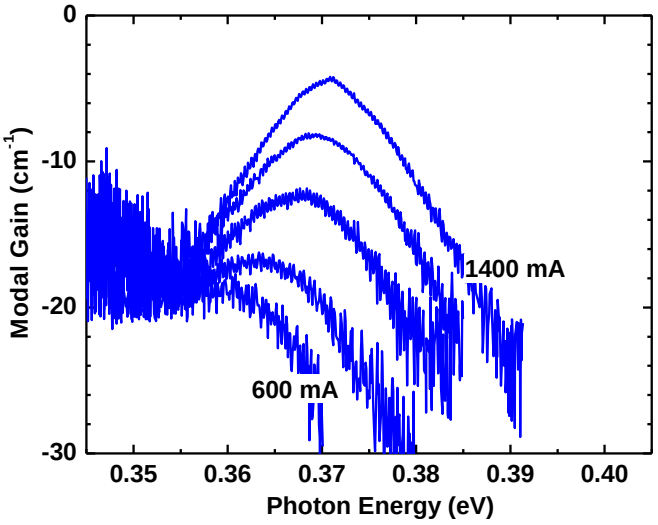

Figure 31: Current dependence of the modal gain spectra measured in pulse mode at (200 ns / 2 MHz) 290K for 4-QW, 1-mm-long, 100-μm-wide, uncoated lasers emitting 3.36 μm.

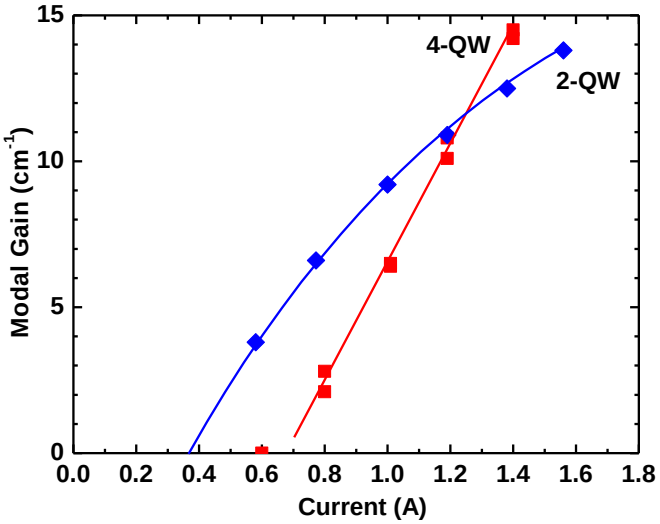

Figure 32: Current dependences of the peak modal gain of 3.36-μm devices with two QWs and four QWs.

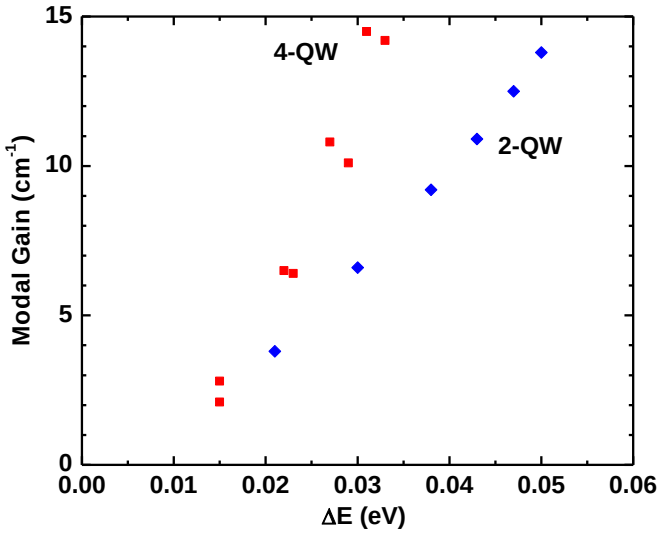

Figure 33: Peak modal gain versus width of modal gain spectra (quasi-Fermi separation of carriers in QWs) for 3.36-μm devices with two QWs and four QWs.

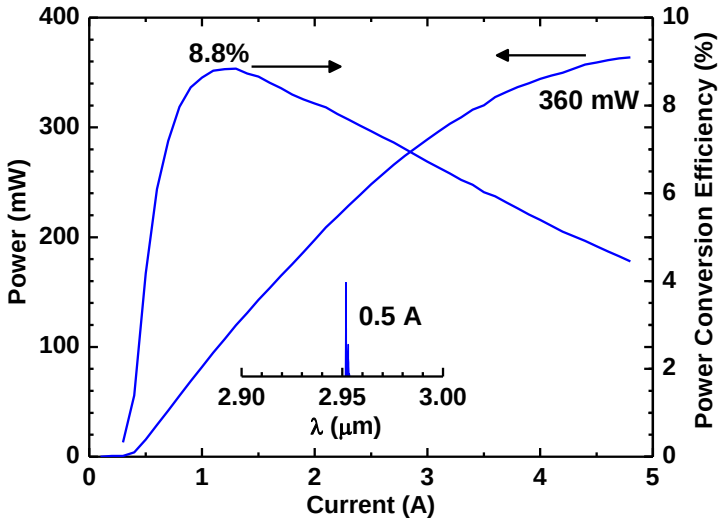

Figure 34: Light-current characteristics measured in CW regime at 17 °C for 2-mm-long, 100-μm-wide, AR/HR coated diode lasers with optimized design and emitting near 3 μm (reference [74]).

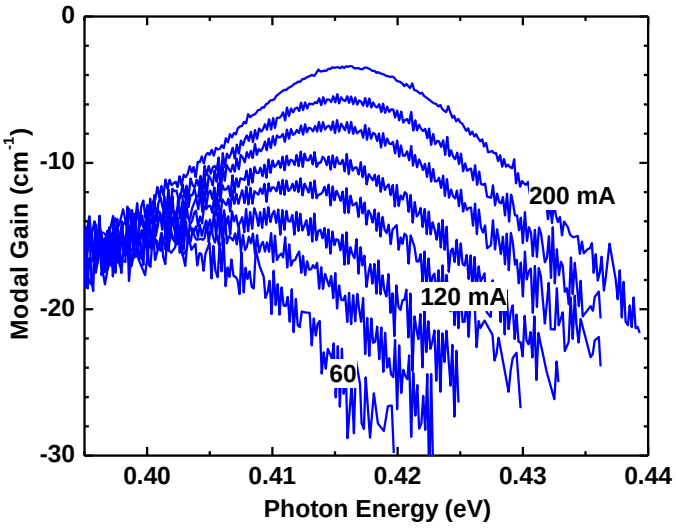

Figure 35: Current dependence of the modal gain spectra measured in pulsed regime (200ns / 2MHz) for 1-mm-long, 100-μm-wide, uncoated lasers emitting 3.0 μm (reference [74]).

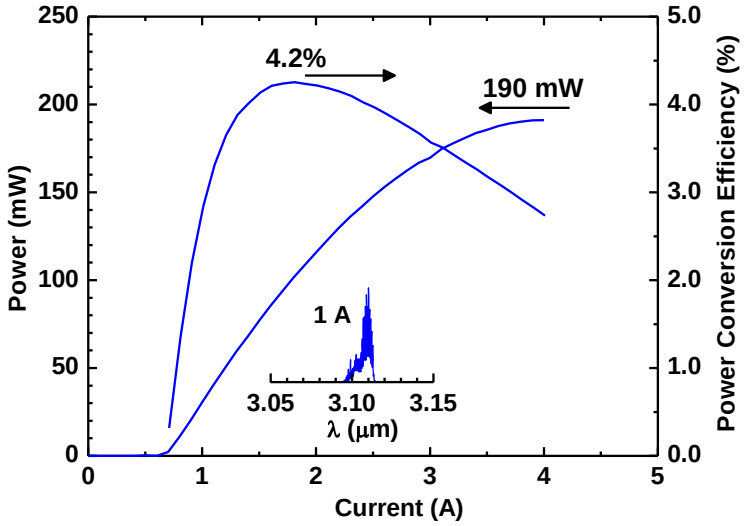

Figure 36: Light-current characteristics measured in CW regime at 17 °C for 2-mm-long, 100-μm-wide, AR/HR coated diode lasers emitting near 3.1 μm (reference [72]).

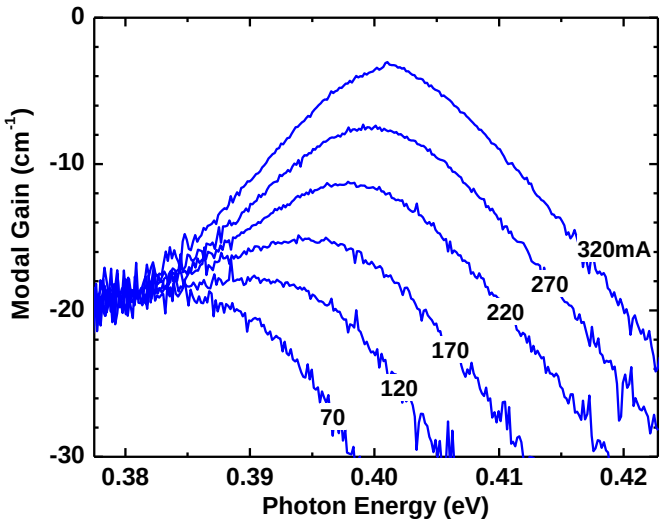

Figure 37: Current dependence of the modal gain spectra measured in pulsed regime (200ns / 2MHz) for 1-mm-long, 100-μm-wide, uncoated lasers emitting 3.1 μm (reference [72]).

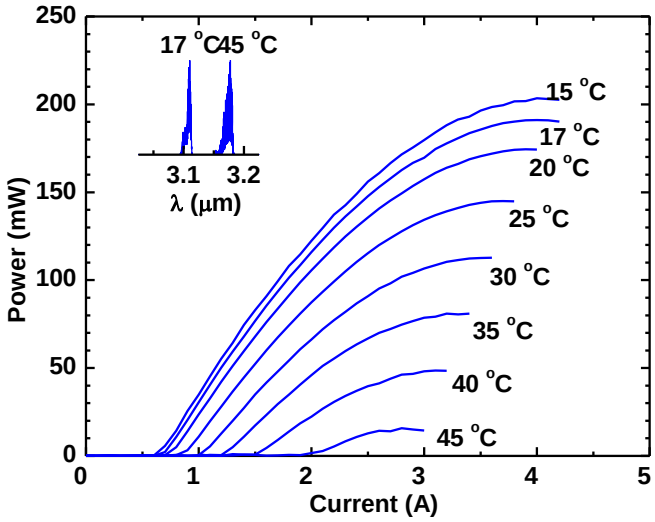

Figure 38: Light-current characteristics measured in CW regime above room temperature for 2-mm-long, 100-μm-wide, AR/HR coated diode lasers emitting near 3.1 μm (reference [72]).

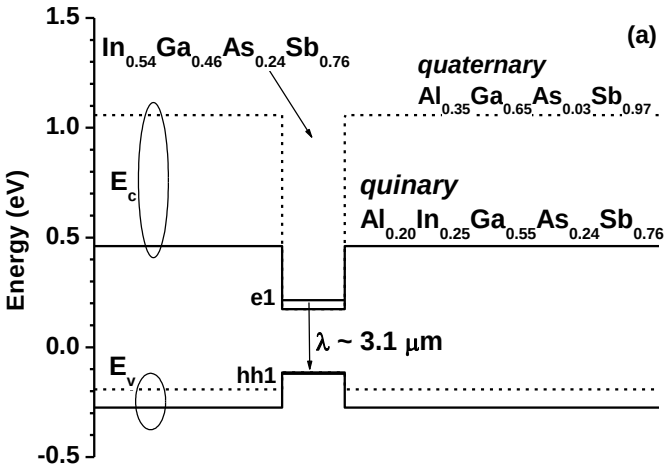

Figure 39a: Calculated band alignment for 3.1 μm emitting lasers. Solid line shows the band edges for QW materials and for quinternary AlInGaAsSb barriers. The dashed line shows the band edge position for quaternary AlGaAsSb alloys.

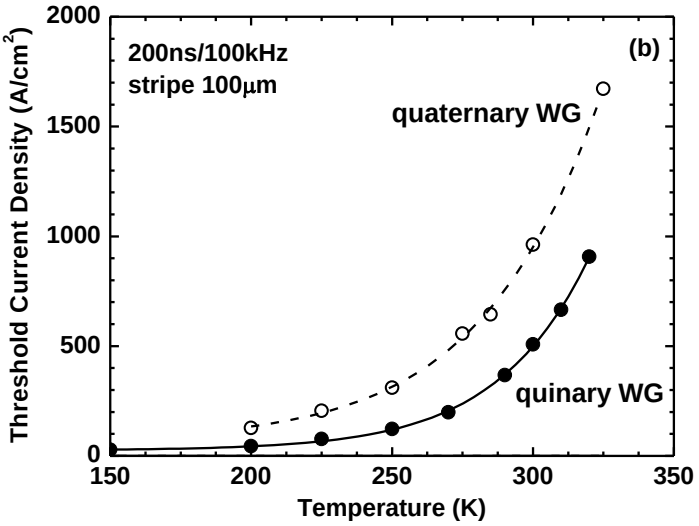

Figure 39b: Temperature dependences of the threshold current density for 3.1 μm emitting lasers with AlGaAsSb quaternary and AlGaInAsSb quinternary barriers.

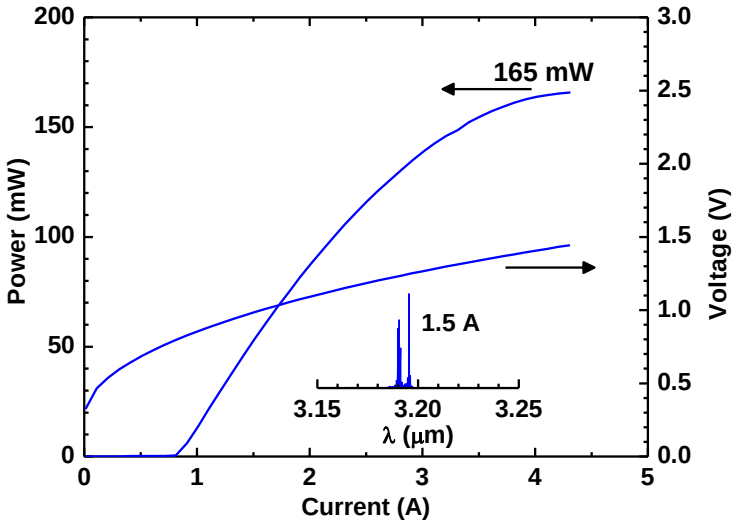

Figure 40: Light-current and voltage-current characteristics measured in CW regime at 17 °C for 2-mm-long, 100-μm-wide, AR/HR coated diode lasers emitting near 3.2 μm (reference [72]).

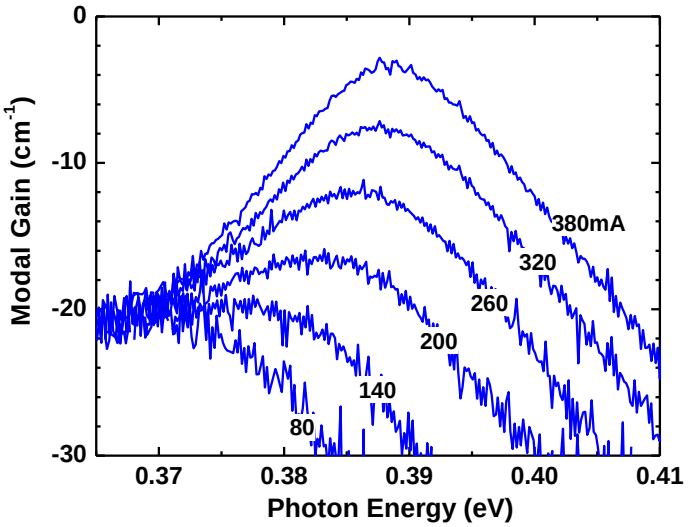

Figure 41: Current dependence of the modal gain spectra measured in pulsed regime (200ns / 2MHz) for 1-mm-long, 100-μm-wide, uncoated lasers emitting 3.2 μm (reference [72]).

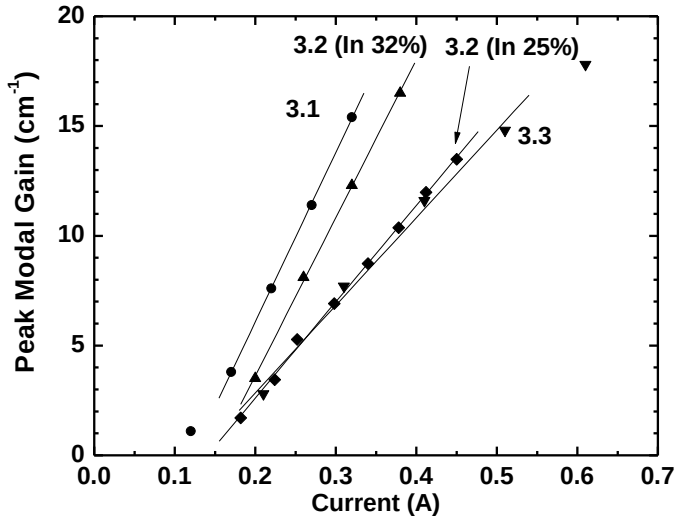

Figure 42: Dependences of the peak modal gain on current of four 1-mm-long, 100-μm-wide, uncoated lasers emitting in spectral region from 3.1 to 3.3 μm at 17 °C (reference [72]).

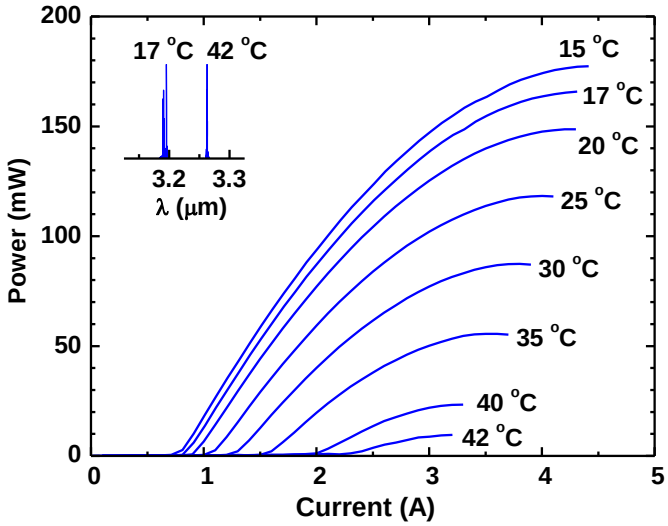

Figure 43: Light-current characteristics measured in CW regime above RT for 2-mm-long, 100-μm-wide, AR/HR coated diode lasers emitting near 3.2 μm (reference [72]).

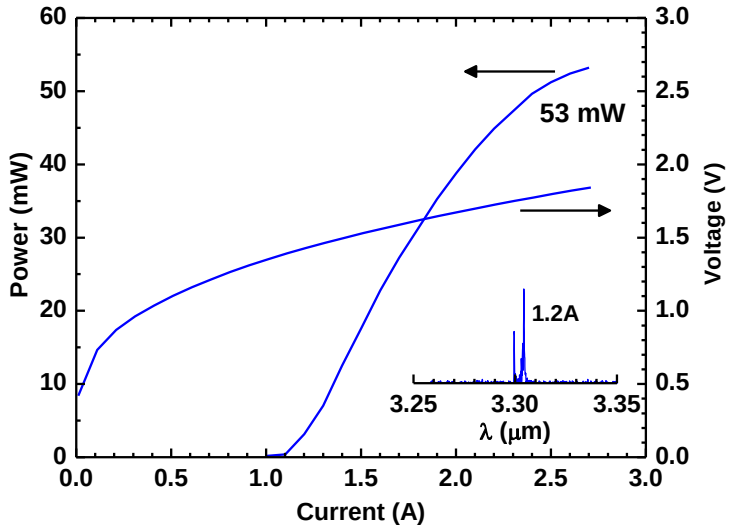

Figure 44: Light-current and voltage-current characteristics measured in CW regime at 17 °C for 2-mm-long, 100-μm-wide, AR/HR coated diode lasers emitting near 3.3 μm (reference [72]).

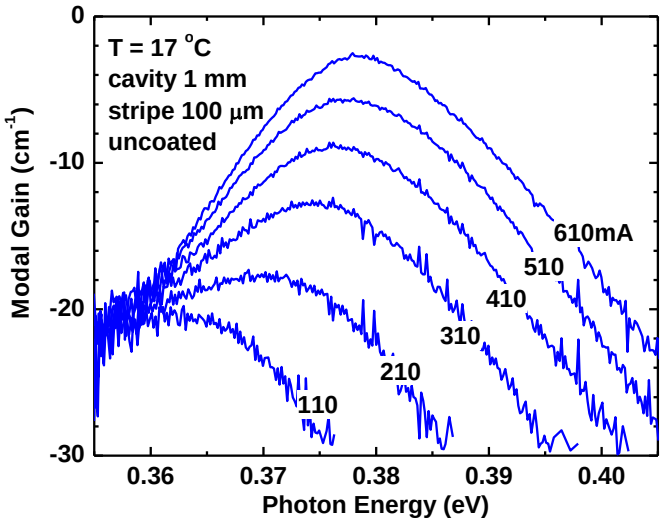

Figure 45: Current dependence of the modal gain spectra measured in pulsed regime (200ns / 2MHz) for 1-mm-long, 100-μm-wide, uncoated lasers emitting 3.4 μm (reference [73]).

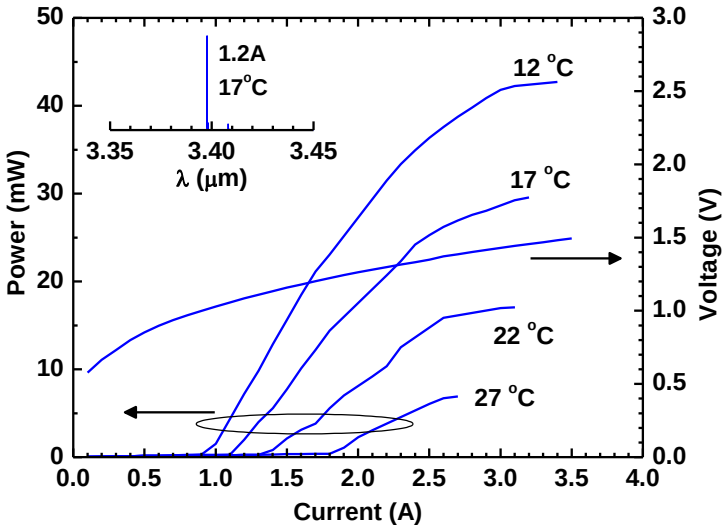

Figure 46: Temperature dependence of light-current characteristics and voltage-current characteristics (17 °C) measured in CW regime for 2-mm-long, 100-μm-wide, AR/HR coated diode lasers emitting near 3.4 μm (reference [73]).

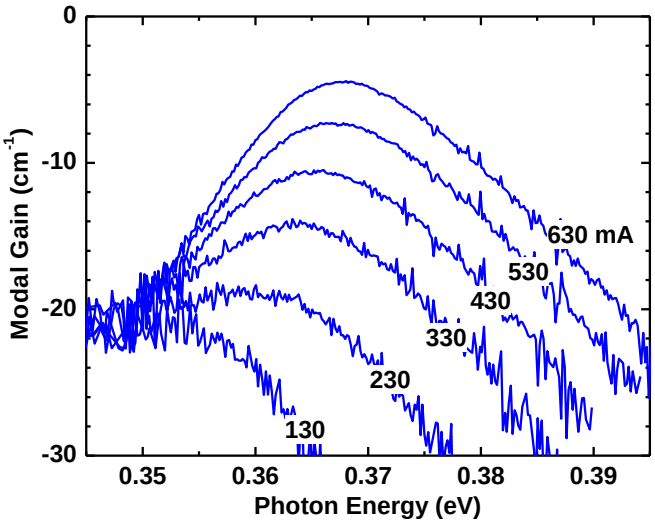

Figure 47: Current dependence of the modal gain spectra measured in pulsed regime (200ns / 2MHz) for 1-mm-long, 100-μm-wide, uncoated diode lasers emitting near 3.4 μm (reference [73]).

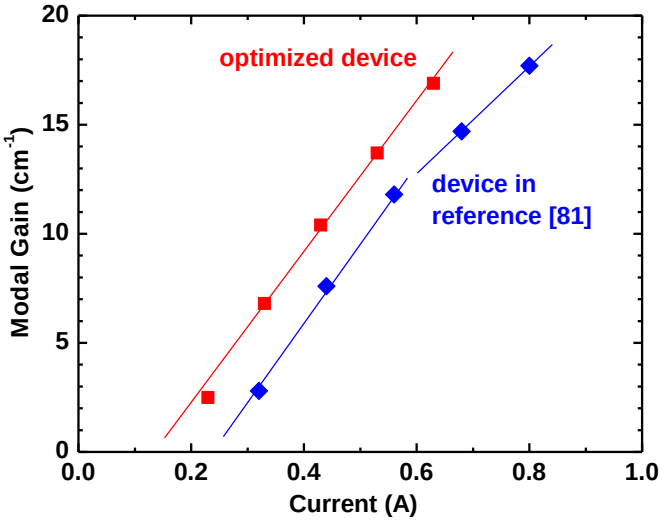

Figure 48: Dependences of the peak modal gain on current of 1-mm-long, 100-μm-wide, uncoated lasers emitting in spectral region from 3.3 to 3.4 μm at 17 °C.

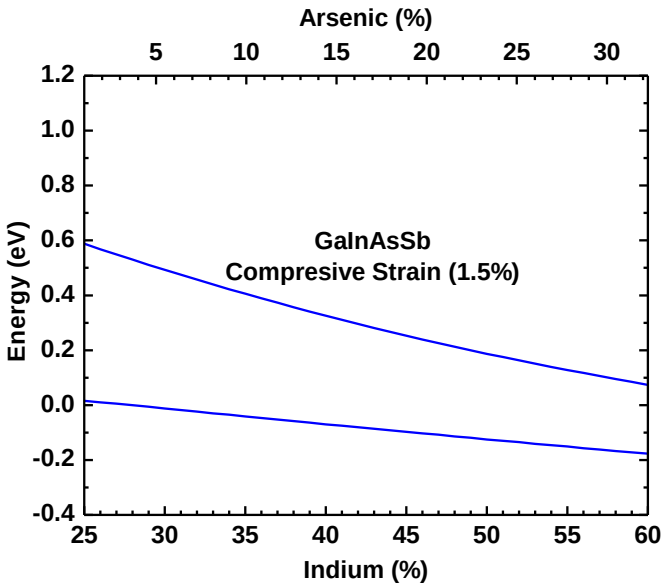

Figure 49: Calculated positions of the band edges on absolute energy scale for GaInAsSb QW alloy with 1.5% compressive strain with respect to GaSb substrate.

Conclusion

The optimization of GaSb-based laser designs described in this dissertation leads to remarkable enhancement of the device differential gain and internal efficiency as well as suppression of the device threshold current density. A major breakthrough in mid-IR GaSb-based diode laser performance was achieved as a result of steady improvement of the conditions of hole localizations in the device QWs. The use of quinternary AlGaInAsSb as barrier material allows to optimize the holes confinement in QWs of devices operated within the spectra region above 3 μm.

Summarizing our efforts (2007-2011) we can conclude that the improvement of device design and utilization of new type of heterostructure materials leads to extension of GaSb-based type-I laser room temperature CW operating wavelength up to 3.45 μm (see Figure 50).

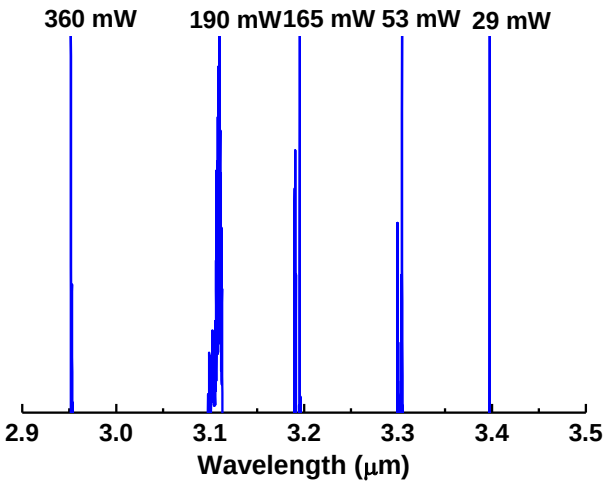

Figure 50: Development of GaSb-based type-I diode lasers emitting above 3 μm

References

1 R. N. Hall, G. E. Fenner, J. D. Kingsley, T. J. Soltys, R. O. Carlson, “Coherent light emission from GaAs junction”, Phys. Rev. Lett., vol. 9, no. 9, pp. 366-368 (1962).

2 M. I. Nathan, W. P. Dumke, G. Burns, F. H. Dill, G. Lasher, “Stimulated emission of radiation from GaAs p-n junctions”, Appl. Phys. Lett., vol. 1, no. 3, pp. 62-64 (1962).

3 T. M. Quist, R. H. Rediker, R. J. Keyes, W. E. Krag, B. Lax, A. L. McWhorter, H. J. Zeigler, “Semiconductor MASER of GaAs”, Appl. Phys. Lett., vol. 1, no. 4, pp. 91-92 (1962).

4 R. Hibst, U. Keller, “Experimental studies of the application of the Er:YAG laser on dental hard substances: I. Measurement of the ablation rate”, Lasers Surg. Med., vol. 9, no. 4, pp. 338-344 (1989).

5 C. Bader, I. Krejci, “Indications and limitations of Er:YAG laser applications in dentistry”, Am. J. Dent., vol. 19, no. 3, pp. 178-186 (2006).

6 A. Vicet, D. A. Yarekha, A Pérona, Y. Rouillard, S. Gaillard, A. N. Baranov, “Trace gas detection with antimonide-based quantum-well diode lasers”, Spectrochimica Acta., vol. 58, no. 11, pp. 2405-2412 (2002).

7 L. S. Rothman, I. E. Gordon, A. Barbe, D. C. Benner, P. F. Bernath, M. Birk, V. Boudon, L. R. Brown, A. Campargue, J. -P. Champion, K. Chance, L. H. Coudert, V. Dana, V. M. Devi, S. Fally, J. -M. Flaud, R. R. Gamache, A. Goldman, D. Jacquemart, I. Kleiner, N. Lacome, W. J. Lafferty, J. -Y. Mandin, S. T. Massie, S. N. Mikhailenko, C. E. Miller, N. Moazzen-Ahmadi, O. V. Naumenko, A. V. Nikitin, J. Orphal, V. I. Perevalov, A. Perrin, A. Predoi-Cross, C. P. Rinsland, M. Rotger, M. Simecková, M. A. H. Smith, K. Sung, S. A. Tashkun, J. Tennyson, R. A. Toth, A. C. Vandaele, J. Vander Auwera, “The HITRAN 2008 molecular spectroscopic database”, J. Quantitative Spectrosc. Radiat. Transf., vol. 110, no. 9-10, pp 533-572139 (2005).

8 J. Wagner, N. Schulz, B. Rösener, M. Rattunde, Q. Yang, F. Fuchs, C. Manz, W. Bronner, C. Mann, K. Köhler, M. Raab, E. Romasev, H. D. Tholl, “Infrared semiconductor lasers for DIRCM applications”, Proc. SPIE, vol 7115, p. 71150A (2008).I. Vurgaftman, J. R. Meyer, L. R. Ram-Mohan, “Band parameters for III-V compound semiconductors and their alloys”, J. Appl. Phys., vol. 89, no. 11, pp. 5815-5875 (2001).

9 I. Vurgaftman, J. R. Meyer, L. R. Ram-Mohan, “Band parameters for III-V compound semiconductors and their alloys”, *J. Appl. Phys.*, vol. 89, no. 11, pp. 5815-5875 (2001).

10 J. Devenson, O. Cathabard, R. Teissier, A. N. Baranov, “High temperature operation of λ≈3.3 μm quantum cascade lasers”, Appl. Phys. Lett., vol. 91, no. 14, p. 141106 (2007).

11 J. Devenson, O. Cathabard, R. Teissier, A. N. Baranov, “InAs/AlSb quantum cascade lasers emitting at 2.75-2.97 μm”, Appl. Phys. Lett., vol. 91, no. 25, p. 251102 (2007).

12 O. Cathabard, R. Teissier, J. Devenson, J. C. Moreno, A. N. Baranov, “Quantum cascade lasers emitting near 2.6 μm”, Appl. Phys. Lett., vol. 96, no. 14, p. 141110 (2010).

13 R. Kaspi, A. P. Ongstad, “High performance optically pumped antimonide lasers operating in the 2.4-9.3 μm wavelength range”, Appl. Phys. Lett., vol. 88, no. 4, p. 041122 (2006).

14 M. Kim, C. L. Canedy, W. W. Bewley, C. S. Kim, J. R. Lindle, J. Abell, I. Vurgaftman, J. R. Meyer, “Interband cascade laser emitting at λ=3.75 μm in continuous wave above room temperature”, Appl. Phys. Lett., vol. 92, no. 19, p. 191110 (2008).

15 I. Vurgaftman, C. L. Canedy, C. S. Kim, M. Kim, W. W. Bewley, J. R. Lindle, J. Abell, J. R. Meyer, “Mid-infrared interband cascade lasers operating at ambient temperatures”, New J. Phys., vol. 11, no. 12, p. 125015 (2009).

16 D. Caffey, T. Day, C. S. Kim, M. Kim, I. Vurgaftman, W. W. Bewley, J. R. Lindle, C. L. Canedy, J. Abell, J. R. Meyer, “Performance characteristics of a continuous-wave compact widely tunable external cavity interband cascade lasers”, Opt. Exp., vol. 18, no. 15, p. 15691 (2010).

17 E. Yablonovitch, E. Kane, “Reduction of lasing threshold current density by the lowering of valence band effective mass,” IEEE J. Lightw. Technol., vol. 4, no. 5, pp. 504-506 (1986).

18 J. Chen, D. Donetsky, L. Shterengas, M. Kisin, G. Kipshidze, G. Belenky, “Effect of Quantum Well Compressive Strain Above 1% On Differential Gain and Threshold Current Density in Type-I GaSb-Based Diode Lasers”, IEEE J. Quantum Electron., vol. 44, no. 12, pp. 1204-1210 (2008).

19 G. P. Donati, R. Kaspi, K. J. Malloy, “Interpolating semiconductor alloy parameters: Application to quaternary III-V band gaps”, J. Appl. Phys., vol. 94, no. 9, pp. 5814-5819 (2003).

20 M. V. Kisin, H. S. El-Ghoroury, “Modeling of injection characteristics of polar and nonpolar III-nitride multiple quantum well structures”, J. Appl. Phys., vol. 107, no. 10, p. 103106 (2010).

21 G. L. Bir, G. E. Pikus, Symmetry and Strain-Induced Effects in Semiconductors, New York, Wiley (1974).

22 M. V. Kisin, R. G. W. Brown, H. S. El-Ghoroury, “Optimum quantum well width for III-nitride nonpolar and semipolar laser diodes”, Appl. Phys. Lett., vol. 94, no. 2, p. 021108 (2009).

23 M. V. Kisin, R. G. W. Brown, H. S. El-Ghoroury, “Optical characteristics of III-nitride quantum wells with different crystallographic orientations”, J. Appl. Phys., vol. 105, no. 1, p. 013112 (2009).

24 A. E. Bochkarev, L. M. Dolginov, A. E. Drakin, L. V. Druzhinina, P. G. Eliseev, and B. N. Sverdlov, “Injection InGaSbAs lasers emitting radiation of wavelengths 19.-2.3μ at room temperature”, Sov. J. Quantum Electron., vol. 15, no. 6, pp. 869-870 (1985).

25 C. Caneau, A. K. Srivastava, A. G. Dentai, J. L. Zyskind, M. A. Pollack, “Room-temperature GaInAsSb/AlGaAsSb DH injection lasers at 2.2 μm”, Electron. Lett., vol. 21, no. 18, pp. 815-817 (1985).

26 A. E. Bochkarev, L. M. Dolginov, A. E. Drakin, P. G. Eliseev, B. N. Sverdlov, “Continuous-wave lasing at room temperature in InGaSbAs/GaAlSbAs injection heterostructures emitting in the spectral range 2.2-2.4 μm”, Sov. J. Quantum Electron., vol. 18, no. 11, pp. 1362-1363 (1988).

27 H. K. Choi, S. J. Eglash, “Room-temperature cw operation at 2.2 μm of GaINAsSb/AlGaAsSb diode lasers grown by molecular beam epitaxy”, Appl. Phys. Lett., vol. 59, no. 10, pp. 1165-1167 (1991).

28 H. K. Choi, S. J. Eglash, “High-power multiple-quantum-well GaInAsSb/AlGaAsSb diode lasers emitting at 2.1 μm with low threshold current density”, Appl. Phys. Lett., vol. 61, no. 10, pp. 1154-1156 (1992).

29 H. K. Choi, G. W. Turner, S. J. Eglash, “High-power GaInAsSb-AlGaAsSb multiple-quantum-well diode lasers emitting at 1.9 μm”, IEEE Photon. Technol. Lett., vol. 6, no. 1, pp. 7-9 (1994).

30 D. Z. Garbuzov, R. U. Martinelli, H. Lee, R. J. Menna, P. K. York, L. A. DiMarco, M. G. Harvey, R. J. Matarese, S. Y. Narayan, J. C. Connolly, “4 W quasi-continuous-wave output power from 2 μm AlGaAsSb/InGaAsSb single-quantum-well broadened waveguide laser diodes”, Appl. Phys. Lett., vol. 70, no. 22, pp. 2931-2933 (1997).

31 T. Newell, X. Wu, A. L. Gray, S. Dorato, H. Lee, L. F. Lester, “The effect of increased valence band offset on the operation of 2 μm GaInAsSb-AlGaAsSb lasers”, IEEE Photon. Technol. Lett., vol. 11, no. 1, pp. 30-32 (1999).

32 D. Z. Garbuzov, H. Lee, V. Khalfin, R. Martinelli, J. C. Connoly, G. L. Belenky, “2.3-2.7 μm room temperature CW operation of InGaAsSb/AlGaAsSb broad waveguide SCH-QW diode lasers”, IEEE Photon. Technol. Lett., vol. 11, no. 7, pp. 794-796 (1999).

33 Y. Rouillard, F. Genty, A. Perona, A. Vicet, D.A. Yarekha, G. Boissier, P. Grech, A.N. Baranov, C. Alibert, “Edge and vertical surface emitting lasers around 2.0-2.5 μm and their applications”, Phil. Trans. R. Soc. London A, vol. 359, no. 1, pp. 581-597 (2001).

34 M. Rattunde, J. Schmitz, R. Kiefer, J. Wagner, “GaSb-based 2.X μm quantum-well diode lasers with low beam divergence and high output power”, Appl. Phys. Lett., vol. 88, no. 8, p. 081115 (2006).

35 C. Mermelstein, S. Simanowski, M. Mayer, R. Kiefer, J. Schmitz, M. Walther, J. Wagner, “Room-temperature low-threshold low-loss continuous-wave operation of 2.26 μm GaInAsSb/AlGaAsSb quantum-well laser diodes”, Appl. Phys. Lett,, vol. 77, no. 11, pp. 1581-1583 (2000).

36 M. Garcia, A. Salhi, A. Pérona, Y. Rouillard, C. Sirtori, X. Marcadet, C. Alibert, “Low threshold high-power room-temperature continuous-wave operation diode laser emitting at 2.26 μm”, Photon. Technol. Lett., vol. 16, no. 5, pp. 1253-1255 (2004).

37 D. Donetsky, G. Kipshidze, L. Shterengas, T. Hosoda, G. Belenky, “2.3-μm type-I quantum well GaInAsSb/AlGaAsSb/GaSb laser diodes with a quasi-CW output power of 1.4 W”, Electron. Lett., vol. 43, no. 15, pp. 810-811 (2007).

38 J. G. Kim, L. Shterengas, R. U. Martinelli, G. L. Belenky, D. Z. Garbuzov, W. K. Chan, “Room-temperature 2.5 μm InGaAsSb/AlGaAsSb diode lasers emitting 1 W continuous-wave”, Appl. Phys. Lett., vol. 81, no. 17, pp. 3146-3148 (2002).

39 J. G. Kim, L. Shterengas, R. U. Martinelli, G. L. Belenky, “High-power room-temperature continuous wave operation of 2.7- and 2.8 μm In(Al)GaAsSb/GaSb diode lasers”, Appl. Phys. Lett., vol. 83, no. 10, pp. 1926-1928 (2003).

40 H. K. Choi, J. N. Walpole, G. W. Turner, M. K. Connors, L. J. Missaggia, M. J. Manfra, “GaInAsSb–AlGaAsSb tapered lasers emitting at 2.05 μm with 0.6-W diffraction-limited power”, IEEE Photon. Technol. Lett., vol. 10, no. 7, pp. 938-940 (1998).

41 J. N. Walpole, H. K. Choi, L. J. Missaggia, Z. L. Liau, M. K. Connors, G. W. Turner, M. J. Manfra, C. C. Cook, “High-power high-brightness GaInAsSb-AlGaAsSb tapered laser arrays with anamorphic collimating lenses emitting at 2.05 μm”, IEEE Photon. Technol. Lett., vol. 11, no. 10, pp. 1223-1225 (1999).

42 H. K. Choi, S. J. Eglash, M. K. Connors, “Single-frequency GaInAsSb/AGaAsSb quantum-well ridge-waveguide lasers emitting at 2.1 μm”, Appl. Phys. Lett., vol. 63, no. 24, pp. 3271-3272 (1993).

43 D.A. Yarekha, G. Glastre, A. Perona, Y. Rouillard, F. Genty, E.M. Skouri, G. Boissier, P. Grech, A. Joullie, C. Alibert, A.N. Baranov, “High temperature GaInSbAs/GaAlSbAs quantum well singlemode continuous wave lasers emitting near 2.3 μm”, Electron. Lett., vol. 36, no. 6, pp. 537-539 (2000).

44 J. Wang, M. Maiorov, D.S. Baer, D.Z. Garbuzov, J.C. Connolly, R.K. Hanson, “In situ combustion measurements of CO with diode-laser absorption near 2.3 μm”, Appl. Opt., vol. 39, no. 30, pp. 5579-5589 (2000).

45 A. Salhi, D. Barat, D. Romanini, Y. Rouillard, A. Ouvrard, R. Werner, J. Seufert, J. Koeth, A. Vicet, A. Garnache, “Single-frequency Sb-based distributed-feedback lasers emitting at 2.3 μm above room temperature for application in tunable diode laser absorption spectroscopy”, Appl. Opt., vol. 45, no. 20, pp. 4957-4965 (2006).

46 M. Hümmer, K. Rößner, A. Benkert, A. Forchel, “GaInAsSb-AlGaAsSb distributed feedback lasers emitting near 2.4 μm”, IEEE Photon. Technol. Lett., vol. 16, no. 2, pp. 380-382 (2004).

47 J. A. Gupta, P. J. Barrios, J. Lapointe, G. C. Aers, C. Storey, “Single-mode 2.4 μm InGaAsSb/AlGaAsSb distributed feedback lasers for gas sensing”, Appl. Phys. Lett., vol. 95, no. 4, p. 041104 (2009).

48 K. Rößner, M. Hümmer, A. Benkert, A. Forchel, “Long-wavelength GaInAsSb/AlGaAsSb DFB lasers emitting near 2.6 μm”, Physica E, vol. 30, no. 1-2, pp. 159-163 (2005).

49 M. Hümmer, K. Rößner, T. Lehnhardt, M. Müller, A. Forchel, R. Werner, M. Fischer, J. Koeth, “Long wavelength GaInAsSb-AlGaAsSb distributed-feedback lasers emitting at 2.84 μm”, Electron. Lett., vol. 42, no. 10, pp. 583-584 (2006).

50 T. Lehnhardt, M. Hümmer, K. Rößner, M. Müller, S. Höfling, A. Forchel, “Continuous wave single mode operation of GaInAsSb/GaSb quantum well lasers emitting beyond 3 μm”, Appl. Phys. Lett., vol. 92, no. 18, p. 183508 (2008).

51 A. N. Baranov, Y. Rouillard, G. Boissier, P. Grech, S. Gaillard, C. Alibert, “Sb-based monolithic VCSEL operating near 2.2 μm at room temperature”, Electron. Lett., vol. 34, no. 3, pp. 281-282 (1998).

52 A. Bachmann, T. Lim, K. Kashani-Shirazi, O. Dier, C. Lauer, M. -C. Amann, “Continuous-wave operation of electrically pumped GaSb-based vertical cavity surface emitting laser at 2.3 μm”, Electron. Lett., vol. 44, no. 3, pp. 202-203 (2008).

53 L. Cerutti, A. Ducanchez, P. Grech, A. Garnache, F. Genty, “Room-temperature, monolithic, electrically-pumped type-L quantum-well Sb-based VCSELs emitting at 2.3 μm”, Electron. Lett., vol. 44, no. 3, pp. 203-204 (2008).

54 A. Ducanchez, L. Cerutti, P. Grech, F. Genty, “Room-temperature continuous-wave operation of 2.3-μm Sb-based electrically pumped monolithic vertical-cavity lasers”, IEEE Photon. Technol. Lett., vol. 20, no. 20, pp. 1745-1747 (2008).

55 A. Bachmann, S. Arafin, K. Kashani-Shirazi, “Single-mode electrically pumped GaSb-based VCSELs emitting continuous-wave at 2.4 and 2.6 μm”, New J. Phys., vol. 11, no. 12, p. 125014 (2009).

56 B. Roesener, M. Rattunde, R. Moser, C. Manz, K. Koehler, J. Wagner, “GaSb-based optically pumped semiconductor disk laser using multiple gain elements”, IEEE Photon. Technol. Lett., vol. 21, no. 13, pp. 848-850 (2009).

57 B. Roesener, N. Schulz, M. Rattunde, C. Manz, K. Koehler, J. Wagner, “High-power high-brightness operation of a 2.25-μm (AlGaIn)(AsSb)-based barrier-pumped vertical-external-cavity surface-emitting laser”, IEEE Photon. Technol. Lett., vol. 20, no. 7, pp. 502-504 (2008).

58 B. Roesener, M. Rattunde, R. Moser, S. Kaspar, T. Toepper, C. Manz, K. Koehler, J. Wagner, “Continuous-wave room-temperature operation of a 2.8 μm GaSb-based semiconductor disk laser”, Opt. Lett., vol. 36, no. 3, pp. 319-321 (2011).

59 J. Paajaste, S. Suomalainen, R. Koskinen, A. Harkonen, M. Guina, M. Pessa, “High-power and broadly tunable GaSb-based optically pumped VECSELs emitting near 2 μm”, J. Crystal Growth, vol. 311, no. 7, pp. 1917-1919 (2009).

60 M. Grau, C. Lin. M. -C. Amann, “Low threshold 2.72 μm GaInAsSb/AlGaAsSb multiple-quantum-well laser”, Electron. Lett., vol. 38, no. 25, pp. 1678-1679 (2002).

61 L. Shterengas, G. L. Belenky, J. G. Kim, R. U. Martinelli, “Design of high-power room-temperature continuous-wave GaSb-based type-I quantum-well lasers with λ > 2.5 μm”, Semicond. Sci. Technol., vol. 19, no. 5, pp. 655-658 (2004).

62 M. Grau, C. Lin, O. Dier, M. -C. Amann, “Continuous-wave GaInAsSb/AlGaAsSb type-I double quantum well lasers for 2.96 μm wavelength”, Electron. Lett., vol. 39, no. 25, pp. 1816-1817 (2003).

63 C. Lin, M. Grau, O. Dier, M. -C. Amann, “Low threshold room-temperature continuous-wave operation of 2.24-3.04 μm GaInAsSb/AlGaAsSb quantum-well lasers”, Appl. Phys. Lett., vol. 84, no. 25, pp. 5088-5090 (2004).

64 L. Shterengas, G. Belenky, G. Kipshidze, T. Hosoda, “Room temperature operated 3.1 μm type-I GaSb-based diode lasers with 80 mW continuous-wave output power”, Appl. Phys. Lett., vol. 92, no. 17, p. 171111 (2008).

65 G. Sek, M. Motyka, K. Ryczko, F. Janiak, J. Misiewicz, S. Belahsene, G. Boissier, Y. Rouillard, “Band offsets and photoluminescence thermal quenching in mid-Infrared emitting GaInAsSb quantum wells with quinary AlGaInAsSb barriers”, Jap. J. Appl. Phys., vol. 49, p. 031202 (2010).

66 M. Motyka, G. Sek, K. Ryczko, J. Misiewicz, S. Belahsene, G. Boissier and Y. Rouillard, “Optical transitions and band gap discontinuities of GaInAsSb/AlGaAsSb quantum wells emitting in the 3 μm range determined by modulation spectroscopy”, J. Appl. Phys., vol. 106, no. 6, p. 066104 (2009).

67 G. Raino, A. Salhi, V. Tasco, R. Intartaglia, R. Cingolani, Y. Rouillard, E. Tournie, M. De Giorgi, “Subpicosecond timescale carrier dynamics in GaInAsSb/AlGaAsSb double quantum wells emitting at 2.3 μm”, Appl. Phys. Lett., vol. 92, no. 10, p. 101931 (2008).

68 M. Grau, C. Lin, O. Dier, C. Lauer, M. -C. Amann, “Room-temperature operation of 3.26 μm GaSb-based type-I lasers with quinternary AlGaInAsSb barriers”, Appl. Phys. Lett., 87, no. 24, p. 241104 (2005).

69 L. Shterengas, G. Kipshidze, T. Hosoda, J. Chen, G. Belenky, “Diode lasers emitting at 3 μm with 300 mW of continuous-wave output power”, Electron. Lett., vol. 45, no. 18, pp. 942-943 (2009).

70 J. A. Gupta, P. J. Barrios, G. C. Aers, P. Waldron, C. Storey, “Room-temperature continuous-wave operation of type-I GaSb-based lasers at 3.1 μm” Electron. Lett., vol. 45, no. 16, pp. 835-837 (2009).

71 J. A. Gupta, B. F. Ventrudo, P. Waldron, P. J. Barrios, “External cavity tunable type-I diode laser with continuous-wave singlemode operation at 3.24 μm”, Electron. Lett., vol. 46, no. 17, pp. 1218-1220 (2010).

72 T. Hosoda, G. Kipshidze, G. Tsvid, L. Shterengas, G. Belenky, “Type-I GaSb-based laser diodes operating in 3.1- to 3.3-μm wavelength range”, IEEE Photon. Technol. Lett., vol. 22, no. 10, pp. 718-720 (2010).

73 T. Hosoda, G. Kipshidze, L. Shterengas, G. Belenky, “Diode lasers emitting near 3.44 μm in continuous-wave regime at 300K”, Electron. Lett., vol. 46, no. 21, pp. 1455-1457 (2010).

74 G. Belenky, L. Shterengas, G. Kipshidze, T. Hosoda, "Type-I diode lasers for spectral region above 3 μm", IEEE J. Sel. Topics Quantum Electron., vol. 17, no. 5, pp. 1426-1434 (2011).

75 T. Hosoda, G. Belenky, L. Shterengas, G. Kipshidze, M. V. Kisin, “Continuous-wave room temperature operated 3.0 μm type I GaSb-based lasers with quinternary AlInGaAsSb barriers”, Appl. Phys. Lett., vol. 92, no. 9, p. 091106 (2008).

76 J. Chen, G. Kipshidze, L. Shterengas, T. Hosoda, Y. Wang, D. Donetsky, G. Belenky, “2.7-μm GaSb-based diode lasers with quinary waveguide”, IEEE Photon. Technol. Lett., vol. 21, no. 16, pp. 1112-1114 (2009).

77 T. Hosoda, G. Kipshidze, L. Shterengas, S. Suchalkin, G. Belenky, “200 mW type I GaSb-based laser diodes operating at 3 μm: Role of waveguide width”, Appl. Phys. Lett., vol. 94, no. 26, p. 261104 (2009).

78 P. A. Dementyev, M. S. Dunaevskii, A. V. Ankudinov, I. V. Makarenko, V. N. Petrov, A. N. Titkov, A. N. Baranov, D. A. Yarekha, R. Laiho, “Giant oxidation related relief of Al-rich layers on cleaved mirrors of GaSb/$Ga_{0.1}Al_{0.9}$SbAs/GaInAsSb layer structures”, Appl. Phys. Lett., vol. 89, no. 8, p. 081103 (2006).

79 S. Adachi, “Band gaps and refractive indices of AlGaAsSb, GaInAsSb, and InPAsSb: Key properties for a variety of the 2-4-μm optoelectronic device applications”, J. Appl. Phys., vol. 61, no. 10, pp. 4869-4876 (1987).

80 B. S. Ryvkin, E. A. Avrutin, “Effect of carrier loss through waveguide layer recombination on the internal quantum efficiency in large-optical-cavity laser diodes”, Appl. Phys. Lett., vol. 97, no. 11, p. 113106 (2005).

81 L. Shterengas, G. Belenky, T. Hosoda, G. Kipshidze, S. Suchalkin, “Continuous wave operation of diode lasers at 3.36 μm at 12 °C”, Appl. Phys. Lett., vol. 93, no. 1, p. 011103 (2008).

Appendix: Measurement of the optical gain

One of the most important parameters relating the physical properties of the semiconductor structure to output characteristics of the laser diode is the optical gain. Optical gain and its dependence on the operating conditions determine not only the basic output characteristics, such as threshold current, but also the temperature dependence of the output characteristics, as well high-speed performance of the laser. The wave in the resonator of semiconductor can be written as:

$$E = E_0(y,z)\cdot exp[j(kx-\omega t)]$$

where

$$k = k' + jk'' = \frac{2\pi N_{eff}(\lambda)}{\lambda} - j\frac{1}{2}g(\lambda)$$

N_{eff} is an effective index of refraction for the optical mode, and *g(λ)* is the modal optical gain. The factor of 2 comes in because the optical gain is usually defined with respect to optical power, not optical field intensity.

Modal optical gain *g(λ)* is related to the material optical gain *G(λ)*:

$$g(\lambda) = \Gamma G(\lambda)$$

where Γ is optical confinement factor (the fraction of the transverse optical mode overlapping the active layer and therefore experiencing optical gain) and α_{tot} is total optical loss which consists of the mirror loss and internal loss (usually attributed to free carrier absorption and scattering from waveguide imperfections:

$$\alpha_{tot} = \alpha_m + \alpha_{int} = \frac{1}{L}ln\left(\frac{1}{R}\right) + \alpha_{int}$$

where the mirror loss is $\frac{1}{L}ln\left(\frac{1}{R}\right)$ with the cavity length L and $R = \sqrt{R_1 R_2}$ (geometrical mean of the mirror reflectivities).

Optical gain can be extracted from both amplified spontaneous emission (ASE) and true spontaneous emission (TSE), as well as using some other methods, such as direct transmission measurement or variable stripe length (VSL) technique. Direct transmission measurement may be advantageous when both facets are anti-reflection (AR) coated (mirror loss is very high) and Fabry-Perot contrast is very small. VSL technique has an advantage of not being influenced by the resonator quality. However it requires a special sample preparation and cannot be used for a single device.

A cleaved mirrors forming the Fabry-Perot resonator creates a very clean interference pattern, which is used to analyze the optical gain. Following equation describes the dependence of the ASE intensity on the wavelength in the approximation of uniform gain inside the laser cavity:

$$I(\lambda) = \frac{B(1+R\cdot exp[(\Gamma G-\alpha_{int})L])(1-R)}{(1+R\cdot exp[(\Gamma G-\alpha_{int})L])^2 - 4R\cdot exp[(\Gamma G-\alpha_{int})L]sin^2\left(\frac{2\pi\pi L}{\lambda}\right)}$$

where *B* is the proportionality coefficient equal to the total amount of ASE coupled into the lasing mode.

B. Hakki and T.Paoli proposed to determine the modal optical gain from the contrast of the ASE spectra. The modal optical gain is expressed as:

$$g(\lambda)=\frac{1}{L}ln\frac{\sqrt{r(\lambda)}-1}{\sqrt{r(\lambda)}+1}$$

where $r(\lambda)$ is the peak-to-valley ratio:

$$r(\lambda)=\frac{I_{max}(\lambda)}{I_{min}(\lambda)}$$

An alternative way of determining the optical gain was first proposed by V. Gribkovskii and V. Samoilyukovich and has been extended for many applications by C. Henry et al. It was later used by P. Blood et al. as part of simultaneous analysis of optical gain and recombination based on TSE measurements.

This method is based on the general relations between the rates of spontaneous emission, stimulated emission, and optical absorption. If carriers have Fermi-like distribution functions, the material optical gain is related to the absorption coefficient:

$$G(\varepsilon,\mu,T)=\alpha(\mu,\varepsilon)\cdot\left\{exp\left(\frac{\mu-\varepsilon}{kT}\right)-1\right\}$$

where ε is photon energy, μ is the separation between the quasi-Fermi levels of electrons and holes, and $\alpha(\varepsilon,\mu)$ is the absorption coefficient of the material of the active layer. Generally, $\alpha(\varepsilon,\mu)$ itself depends on the band filling and, therefore, on μ. The relation between spontaneous emission $I_{sp}(\varepsilon)$ and the absorption coefficient is:

$$I_{sp}(\varepsilon)\propto\varepsilon^2\cdot\alpha(\varepsilon,\mu)\cdot exp\left(\frac{\mu-\varepsilon}{kT}\right)$$

By combining the two equations above,

$$G(\varepsilon,\mu,T)\propto\frac{I_{sp}(\varepsilon)}{\varepsilon^2}\cdot\left\{1-exp\left(\frac{\varepsilon-\mu}{kT}\right)\right\}$$